Energy Conversion and Management 144 (2017) 69–87

Contents lists available at ScienceDirect

Energy Conversion and Management

journal homepage: www.elsevier.com/locate/enconman

Comparative analysis of two hybrid energy storage systems used in a two front wheel driven electric vehicle during extreme start-up and regenerative braking operations

Khaled Itani [a], Alexandre De Bernardinis [b,*], Zoubir Khatir [b], Ahmad Jammal [c]

[a] ISAE Cnam Liban, Beirut, Lebanon
[b] SATIE TEMA, IFSTTAR, Versailles, France
[c] Ministry of Higher Education, Beirut, Lebanon

ARTICLE INFO

Article history:
Received 26 January 2017
Received in revised form 22 March 2017
Accepted 8 April 2017
Available online 20 April 2017

Keywords:
Electric vehicle
Hybrid energy storage
Traction control system
Regenerative braking system
Ultracapacitor
Flywheel energy system

ABSTRACT

This paper presents the comparative study of two hybrid energy storage systems (HESS) of a two front wheel driven electric vehicle. The primary energy source of the HESS is a Li-Ion battery, whereas the secondary energy source is either an ultracapacitor (UC) or a flywheel energy system (FES). The main role of the secondary source is to deliver/recover energy during high peak power demand, but also to increase battery lifetime, considered among the most expensive items in the electric vehicle. As a first step, a techno-economic comparative study, supported by strong literature research, is performed between the UC and the FES. The design and sizing of each element will be presented. The comparison criteria and specifications are also described. The adopted approach in this paper is based on an academic non-oriented point of view. In a second step, each of the HESS will be integrated in a more global Simulink model which includes the vehicle model, the traction control system (TCS), the regenerative braking system and the vehicle actuators. Simulation tests are performed for an extreme braking and vehicle starting-up operations. Tests are realized on two different surface road types and conditions (high and low friction roads) and for different initial system states. In order to show the most appropriate storage system regarding compactness, weight and battery constraints minimization, deep comparative analysis is provided.

1. Introduction

Since 2004, the number of electric vehicle (EV) manufacturers has substantially increased, motivated by three majors factors which are the industry, the technology and the market [1]. From a technological point of view, the constraints related to the acceptance of electric vehicles by the public consist of a restricted autonomy of the vehicle and a lack of developed infrastructure (charging terminals, standardization of accessories, sales channels and distribution, technical support, after-sales service, spare parts...). The research and development efforts carried out on batteries, fuel cells and other alternative energy source have direct effects on the autonomy issue [2]. On the other hand, the climate changing (estimated average temperature raising of 6 °C by 2050 [3] and atmospheric concentration of greenhouse gases [4]) is another incentive for researchers and users to elaborate and encourage the clean energy approach.

Thanks to what has been cited above, adding also the technological advances, the scarcity of oil as well as economic and strategic reasons (energy consumption, energy independence strategy), the electric vehicle industry resumes its emergence. This recovery stands on seven main pillars: (1) improvement in battery technologies [2], (2) rise of infrastructure [5,6], (3) commercial offer in evolution, (4) a further partnership between manufacturers, (5) an almost final conclusion for manufacturers stating that the electric vehicle could represent a larger market share in the future, which encouraged competition and therefore investment at all levels, (6) technology sponsored by the governments [7], and laws [8,9], (7) a more mastered technology which led the most reluctant manufacturers [10] to announce their presence in the market for e-mobility.

Energy storage elements for electric vehicles have their share portion in the technological advances. As primary energy storage, the battery has a high energy density but a low power density. The use of other energy storage elements with a high power den-

* Corresponding author.
E-mail addresses: khaled.itani@lecnam.net (K. Itani), alexandre.de-bernardinis@ifsttar.fr (A. De Bernardinis), zoubir.khatir@ifsttar.fr (Z. Khatir), ajammal@higher-edu.gov.lb (A. Jammal).

http://dx.doi.org/10.1016/j.enconman.2017.04.036
0196-8904/

Nomenclature

Vehicle design variables and parameters

m	mass of the vehicle
r	wheel radius
L	wheelbase of the vehicle
l_r (respectively l_f)	distance of the rear (respectively front) wheel axle to the center of mass of the vehicle
h_g	distance from the ground to the center of mass of the vehicle
E_{ke}	kinetic energy of the vehicle
V	vehicle velocity

Cinematic variables

μ_{max}	maximal friction coefficient for a certain road
λ_i	slip coefficient of the wheel i
λ_{max}	slip coefficient corresponding to a maximal friction coefficient
β_{hb-max}	ratio between friction front force and total friction force assuring maximal front/rear braking ratio

Ultracapacitor electrical variables and parameters

U_{c0}	voltage across capacitor
U_{c0min}	ultracapacitor minimal voltage
U_{c0max}	ultracapacitor maximal voltage
I_{c0}	ultracapacitor current
C_0	ultracapacitor capacitance
P_0	ultracapacitor maximal power
ΔE_{UC}	total energy to be recovered from an UC
E_{UC}	energy capacity of the UC

Flywheel energy system variables and parameters

T_{FW}	flywheel torque
J_{FW}	moment of inertia of the flywheel
ω	angular rotation speed
r_o	outer radius
r_i	inner radius
h	length of the flywheel cylinder
ρ	rotor material density
σ_r	radial stress
σ_t	tangential stress
ν	poisson ratio
K	shape factor of the flywheel
N_{max}	maximal permissible speed
σ_{tmin}	minimal tensile strength
E	energy stored in the fywheel
E_{FW}	energy capacity of the FES
E_{lim}	energy limit achieved
e_v	kinetic energy per volume
e_m	kinetic energy per unit mass

Flywheel electrical motor variables and parameters

K_w	winding factor
A	specific electric loading
B_{gav}	specific magnetic loading
L_m	length of the machine
D	diameter
D_{in}	inner diameter
D_{out}	outer diameter
N	machine rotational speed
N_c	number of conductors in series per phase
E_v	electromotive force
η	power efficiency
$\cos\varphi$	power factor
P_{kW}	output power
Φ_p	flux per pole
f	frequency
p	number of poles

Abbreviations

ABS	Anti-Lock Braking System
CFT	Clutched Flywheel Transmission
CVT	Continuous Variable Transmission
EDLC	Electric Double Layer Capacitors
ECE	Economic Commission for Europe
ESS	Energy Storage System
EV	Electric Vehicle
FES	Flywheel Energy Storage
FIA	Fédération Internationale de l'Automobile
FW	Flywheel
HESS	Hybrid Energy Storage System
HEV	Hybrid Electric Vehicle
ICE	Internal Combustion Engine
ISG	Integrated Starter Generator
KERS	Kinetic Energy Recovery System
SEI	Solid Electrolyte Interface
SOC	State of Charge
SOE	State of Energy
TCS	Traction Control System
UC	Ultracapacitor
UN	United Nations
WHP	William Hybrid Power

sity, known as secondary energy storage, aims to complement the battery especially in regenerative braking and start up of the vehicle. This substitution will enhance the battery life as well as the dynamic performance of the vehicle. The combination of the two energy storage elements requires power electronics based converters associated with control and measurement instrumentation, known as hybrid energy storage system (HESS). The secondary energy storage could be either a flywheel or an ultracapacitor (UC).

1.1. State of the art

The flywheel and the UC have both draw researchers' attention as a secondary energy storage element. High-speed flywheels are a potential emerging technology with competitive characteristics if compared to established battery and ultracapacitor in certain vehicular applications.

A general presentation of energy storage technologies can be found in [11–14]. Authors in [12] address various aspects such as historical evolution of energy storage systems, technical characteristics and interaction between smart grid and micro-grids applications. For automotive application, authors in [15] make a review on the flywheels used on vehicles. General comparisons with supercapacitors are also treated, in terms of rated power, energy capacity, specific energy, specific power, system weight and cost. The comparison data specifications had been taken from the energy storage elements manufacturers. The comparison is carried out as an apple to apple comparison, without any particular applications. Tables of flywheels research groups and manufacturers are also listed with their fields of interest.

Optimal energy management for a battery assisted by flywheel for EV is being proposed in [16,17]. The flywheel is coupled to the drive line of a continuous variable transmission (CVT). The results

show potential reduction of energy consumption in extra-urban and highway cycles, while reducing battery peak loads during cycles. Similarly on [18], the energy management strategy of a hybrid-electric vehicle is performed. The strategy is based on fuzzy logic rules optimizing the torque distribution between the internal combustion engine (ICE) and the integrated starter generator (ISG) driven by both the flywheel and the ICE crankshaft. Simulations indicate a reduction of the fuel consumption of the vehicle. T-S Fuzzy strategy based power management is also used by [19] taking into account saving calculation during recuperation of an on-board tram vehicle. The discussion centered on profitability of the energy storage system (ESS) based on ultracapacitors. Ultracapacitors energy recovery for urban railway traction systems are treated in [20]. Work in [21] presents the developments and applications of energy storage devices (batteries, flywheels, UCs, and HESS) used in electrified railways, including metro, trains and trams.

A comprehensive review of flywheel energy storage system technology can be found in [22]. Authors present also power electronic interface used in flywheel applications. Regenerative brake converting kinetic energy into another useful form of energy (electrochemical, mechanical, compressed air...) are presented in [23]. Flywheel characterization using average simulation is depicted in [24].

A switched reluctance motor flywheel having an energy content of 280 kJ (60 krpm, 60 kW peak) installed in a Bio-Diesel prototype car is designed in [25]. At present, the limitations of implementing flywheels in vehicles are partly technical (safety requirements), but also economical. These issues have prevented its usage at large scale into common vehicles. Authors in [26] have presented a conceptual design of a flywheel battery with a 200 W h capacity. The design was focused on using commercially available components. Research team in Heilbronn University [27] tested a 26 kW battery powered electric car of 13 kW h range for 11,000 km. By simulation, a flywheel approach has been introduced for range-extension study.

For energy storage purposes, flywheel materials with higher strengths, and lower densities that would allow the flywheel to spin faster are desirable. More efforts have been done on developing composite materials with higher specific tensile strengths leading to stronger rotors and increasing energy storage capacity [28,29].

In [30], a comprehensive techno-economic and physical modeling of flywheel energy storage system is presented. It is made up of a flywheel, a permanent magnet synchronous machine and a power converter. An economic optimization is done on a short-range ship profile. Comparison has been done using three types of flywheels materials. Similarly in [31], the choice is done for supercapacitors, as primary source, for a recharge per trip plug-in-ferry, based on a techno-economic criterion. Authors concluded that the cheapest solution use flywheel, but it is not ready to be integrated into a plug-in ferry due to integration considerations.

Authors in [32] compare high-speed flywheels (with CVT/Clutch powertrain transmission), ultracapacitors, and batteries functioning as the ESS in a fuel cell based HEV on the basis of cost and fuel economy. The ESS handles the transient loads, the fuel-cell only has to provide the average power. The results have shown that when cost and fuel economy were both considered, high-speed flywheels were competitive with batteries and ultracapacitors. Authors in [33] present a comparative study to determine the optimal combination of HESS used on a shipboard power system in order to optimize the voltage and frequency fluctuations caused by the connection of pulsed loads on the AC and DC sides of the system. Various power converter interfaces that can be used for electromechanical energy storage systems are found in [34].

A general comparative study for high power applications including Li-Ion battery, supercapacitors, flywheels and superconducting magnetic energy storage is discussed in [35], in terms of power, energy, cost, life and performance. Authors in [36] treat the problem of the sizing of the Li-Ion battery and UC, as well as the degree of hybridization between the UC power and the battery power for a plug-in HEV. The job has been focused on solving an optimization problem to minimize fuel consumption.

E-mobility is not the only field where ultracapacitors and flywheels technologies are in great competition due to their similar characteristics. Indeed, the area of competition goes to include large scale power grid and backup power applications. Facing the high level of wind energy penetration to the power grid, a greater need to manage the intermittency produced by the wind turbine generator is a must, especially in order to improve stability during normal and transient operations and to damp short-term power oscillations and discontinuities. In particular, supercapacitors are used as energy storage for a doubly fed induction generator (DFIG) to handle the low-voltage ride through (LVRT) operation during faults [37,38]. Authors in [39] inserted a static synchronous compensator (STATCOM) to a DFIG-based wind farm bus. The STATCOM-supercapacitor combination shows its ability to maintain the bus voltage within desired limits during a symmetrical or asymmetrical fault of the power system, showing short-term stability of the system. Other energy storage systems are also used for these types of applications as the superconducting magnetic energy storage system (SMES). In [40], a superconducting fault-current limiter-magnetic energy storage system is used to smooth the output power to limit surge current of a DFIG.

It should be noted that previous research have not provided a direct comparison between high-speed flywheels and ultracapacitors functioning as a secondary energy storage during extreme regenerative braking and start-up on different road types and conditions for a two front wheel-driven electric vehicle. This paper aims to study and analyze that comparison using Matlab/Simulink® software.

1.2. Li-Ion battery constraints

Li-Ion batteries have a higher specific energy density level (75–200 W h/kg) compared to lead acid (35–50 W h/kg), nickel–cadmium (50–60 W h/kg), and nickel metal hydrate batteries (70–97 W h/kg) [41]. Companies such as Panasonic, Tesla, LG Chem and Samsung SDI are heavily investing in the Lithium Nickel Manganese Cobalt Oxide (NMC) and Lithium Nickel Cobalt Aluminum Oxide (NCA) cells battery chemistries.

A Li-Ion battery is composed of a cathode (reduction reaction side), an anode (oxidation reaction side) and an ionic conductor/-electronic insulator (electrolyte) having the main function to provide ions transportation from one electrode to the other. The capacity losses originate mainly in the interface between electrode and electrolyte consisting of a reduction of the electrolyte and the formation of a solid electrolyte interface (SEI) on the negative electrode, leading to battery aging. An oxidation reaction of the electrolyte happens on the positive electrode side. These reactions lead to an increasing cell impedance, capacity losses and lowered rate capability. The temperature rise helps in magnifying the battery deficiencies which could present a security hazard leading to thermal runaway [42].

On the other hand, Li-Ion battery cannot respond to high dynamic power profiles resulting from an acceleration or a regenerative braking since charge transfer occurs through reduction and oxidation reactions. These profiles, if happened, will overstress the battery which negatively affects the longevity of its lifespan. In fact, these actions will cause degradation at the cell level increasing the internal resistance, and having capacity fade as a consequence. Nevertheless, FW or even UC has the power density to sustain the high power needed for relatively short durations.

1.3. System description

The Li-Ion battery is becoming the most installed storage element in electric vehicles. This is due, in first place, to its high energy density (allowing a great distance drive) and, in second place, to the promising technology not yet fully mature.

Nevertheless, for automotive applications, specifically in hard braking and traction maneuvers, this battery presents several weaknesses related to the chemical reactions taking place while charging/discharging. These reactions could lead to capacity fade, lifespan reduction of the battery and in extreme cases to fire hazard. The lifespan reduction will allow a premature replacement of the battery, the most expensive component in the vehicle.

Another interesting point is that the battery is not able to respond to the power requirements recommended by the traction control or the braking control systems during these severe operations.

Considering all the points listed above and in order to minimize the stresses on the battery, it has been found convenient to implement in the energy storage system, a storage element characterized by its ability to provide the necessary power required by the traction and braking systems. This secondary storage element will substitute the battery during extreme power demand. It should also have a high cycle life due to the indefinite number of acceleration/braking operation during a vehicle drive.

Among all the existing storage elements, the UC and the FW are potential candidates to meet the requirements listed above. The two elements are known for their high power density and high cycle life. On the other hand, both present a low energy density, a high acquisition cost and a high self-discharge.

The hybrid energy storage system (HESS) will combine the high energy density storage element (Li-Ion battery), known as primary storage element, and the high power density storage element (UC or FW), known as secondary storage element. The use of power electronic based converters with their associate control systems is needed in order to dispatch the high power flow according to the energy control strategy.

In this paper, the Nissan Leaf® model vehicle is driven by two 30 kW interior permanent magnet synchronous motors (IPMSM) installed in the front wheels. The power flow will be analyzed for two types of HESS and for two types of operation, extreme braking and starting-up. One HESS is composed of Li-Ion battery and an UC, the other of a Li-Ion battery and a FW. Extreme braking conditions correspond to the maximal braking forces that could be applied to the vehicle for a certain road type and condition while ensuring stability and maneuverability, and avoiding wheels locking. Similarly, the starting-up is performed by a maximal acceleration of the vehicle, initially at rest, ensuring a spinning free performance. These two operations are highly dependent on the road surface conditions and types. For these reasons, appropriate HESS (Fig. 1) are the core elements for high efficiency applications and constitute reliable solutions for mobile applications.

The objective of energy management is to specify power distribution between the different sources of energy in the system in order to achieve a certain level of control strategy. These strategies are classified into two categories: heuristic control and optimal control [43]. The heuristic control is based on intuitive strategies, whereas, the optimal control tends to minimize a cost function in order to obtain a certain performance criteria. In the present paper, the objective is to prevent, as much as possible, the charge/discharge of the battery during vehicle start-up and braking maneuvers, in order to reduce the stress on the battery and enhance its capacity and life cycle. The braking/traction control highly depends on the power profile and system state.

The main contribution of the work consists in the design and sizing of the appropriate secondary energy storage element dedicated to the particular application of the paper, whether it be an ultracapacitor or a flywheel. Firstly, the comparison is based on a techno-economic study. Secondly, simulations are performed on model developed by authors. In fact, authors used previous research works concerning several modules of the overall system which will be detailed later. The simulations would allow to analyze the power flow and the HESS behavior according to its design and control demand. After simulation results, a technological comparison would also be carried out. Even though, the complexity of the overall system is obvious, the obtained results, at each step, show the realistic and the coherent aspect of the designed models, demonstrating more and more the functionality of the simulation as a first step to the final prototype. It is important to mention that the comparison performed for the two HESS for the particular automotive application consisting of a 2 front driven wheel vehicle is realized according to a sliding mode traction control and a constrained based braking control.

The paper layout is as follows: An electromechanical analogies between the UC and the FW is carried out in Section 2. In this section, comparison criteria as well as related comparison found in literature are also discussed. Ultracapacitors review, applications and design are treated in Section 3. Section 4 is dedicated to flywheel. This section will contain a comparison interpretation with the designed ultracapacitors results obtained in Section 3. Section 5 describes the complete system model including the vehicle model, the traction/braking control methods, the hybrid energy storage system, the electric motors control methods. Simulation tests are performed, and comparative analyses are provided in Section 6.

2. Flywheel/ultracapacitor analogies

2.1. Electromechanical analogies

The amount of power transferred is the product of two physical quantities, one relative to an effort, the other to a flow:

$$Power = Effort \times Flow \tag{1}$$

As both power variables play an equal role for each energy domain, the force-voltage, known as classical or direct analogy is the most used and is presented by:

$$\begin{cases} Force \triangleq Effort \triangleq Voltage \\ Velocity \triangleq Flow \triangleq Current \end{cases} \tag{2}$$

An UC is an electrical potential energy element. The energy stored has an electrochemical and electrostatic form. Whereas, a FW is a mechanical kinetic energy element. The energy stored has a mechanical form. Table 1 shows the classical analogy between the mechanical and the electrical domains.

An UC establishes a causal relation between the voltage applied at its terminal and the developed current:

$$\frac{dU_{c0}}{dt} = \frac{I_{c0}}{C_0} \tag{3}$$

where C_0 is the UC capacitance. The power recovered or delivered by the ultracapacitor is the product of its voltage by the current. From a control approach, we are able to regulate the current from zero to the value that would ensure a maximal power flow of 60 kW, even at minimal voltage of the ultracapacitor. This was taken as constraint throughout the control design and as specification at the time of the UC sizing. The current is the highest dynamic electrical quantity in the system and, also, the flow variable considered in Eq. (1). Hence, considering the physical characteristics of the UC and the control requirements, the UC is able to deliver/absorb the maximal power of 60 kW, if needed by the braking and traction control systems.

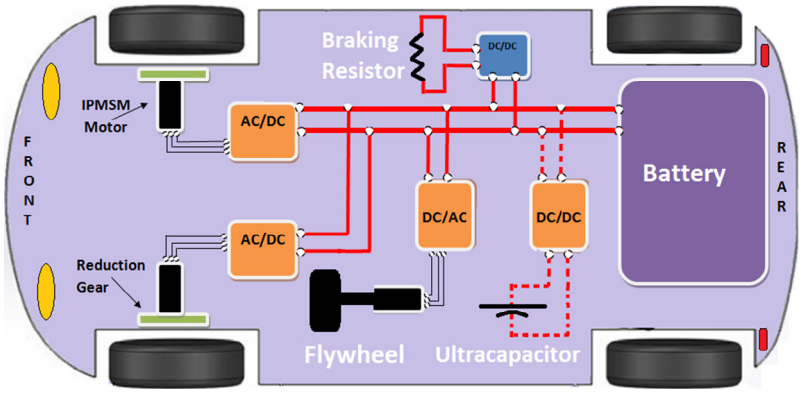

Fig. 1. Vehicle actuators and HESS components having a flywheel or an UC as a secondary storage source.

Table 1
Classical analogy.

Mechanical domain	Electrical domain
Rotational speed	Current
Torque	Voltage
Moment of inertia	Inductance
Damping	Resistor
Spring	Capacitance
Potential energy	Electrostatic energy
Kinetic energy	Magnetic energy

As mentioned, a FW is a rotational kinetic element. Under the action of a torque, a rotational acceleration will take place, as written below:

$$\frac{d\omega}{dt} = \frac{T_{FW}}{J_{FW}} \tag{4}$$

J_{FW} is the moment of inertia and is considered as the mechanical analog of an inductance. The power recovered or delivered by the FW is the product of its torque by the angular rotational speed. From a control point of view, the regulation is done on the torque which is the effort variable considered in Eq. (1). The maximal value of the torque is determined by the magnetic and electromechanical constraints of the electrical machine driving the flywheel. In order to prevent oversizing, the maximal power has been calculated for a maximal torque (22 N m) delivered by the machine. At a certain operating point, the maximal power delivered/absorbed will be limited by the FW speed.

2.2. Comparison criteria

The performance metrics for an electrical energy storage system can be briefed by the cycle efficiency, the cost per unit capacity ($/kW h or $/kW), specific energy (W h/kg), specific power (W/kg), energy density (W h/l), power density (W/l), cycle life, environmental impact including end-of-life disposal cost and safety [2,26].

The battery has shorter cycle life due to unavoidable chemical deterioration (Ref. §I. B). No single type of electrical energy storage element can simultaneously fulfill all the desired characteristics. There will be a need to combine higher energy density insured by the battery, as primary source, with a higher power density energy storage elements, like ultracapacitors or flywheel. Table 2 lists the comparison of technical characteristics of energy storage elements. The data have been collected from different references. It is often to encounter some divergence in values from one reference to another. This issue will be discussed in details more forward, strengthened the argument that the comparison should be performed for a particular application basis.

2.3. Comparison in literature

For an EV, the main role of the secondary energy source is to assist the battery during regenerative braking and vehicle starting up, improve the performance of the system in terms of cost, system life and overall efficiency.

In literature, it is rare to read about ultracapacitors (respectively flywheels) without mentioning flywheels (respectively ultracapacitors), [21,31,32,35,19,44,45]. They have similar specifications in terms of cost, simple measurability of the charge status, low maintenance requirements, high power density, fast response time, suitable for applications with rapid charge and discharge requirements (during braking and acceleration periods). Flywheels are seen to excel in high power applications, placing them closer in functionality to supercapacitors than the batteries [15]. Fig. 2 shows the Ragone plot in terms of high power density energy storage, ultracapacitors and flywheels are situated in a competitive zone.

In electrified railways, flywheels have similar properties to ultracapacitors, but they have a slightly higher charge–discharge time.

Table 2
Technical characteristics of energy storage elements (based from different literature references).

	Battery	Flywheel	UC
Cycle efficiency	>90%	>90%	>90%
Cost per unit capacity	>600 $/kW h	2000–5000 $/kW h	1000–5000 $/kW h
Power density	250–340 W/kg	1–5 kW/kg	0.5–10 kW/kg
Energy density	100–250 W h/kg	10–50 W h/kg	0.5–5 W h/kg
Cycle life	1000–10,000	500,000–1000,000	500,000–1000,000
Environmental impact	Negative	None	Moderate
Self discharge/day	0.1–0.3%	100%	20–40%
Temperature range	−10 °C/45 °C	−30 °C/100 °C	High temperature range
Market availability	Positive	Negative	Positive
Non-moving parts	Positive	Negative	Positive

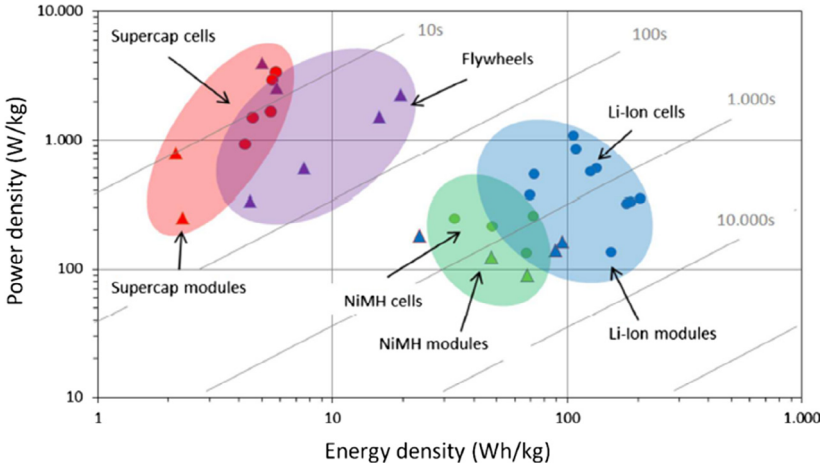

Fig. 2. Ragone plot (related to system mass) [25].

According to [21], stationary flywheels have important dimensions and excessive weight. Onboard flywheels need space in the bogie requiring more space than ultracapacitors. After the diffusion of UCs, the use of flywheels in electrified railways has been reduced because of the superior properties of UCs in terms of maintenance, weight and size [21]. Other authors conclude that flywheel ensures a steady voltage and power level, which is independent of load, temperature and state of charge. In fact the combination battery/flywheel can achieve better performance, regarding voltage fluctuation, than other types of combinations (battery/UC or UC/flywheel), as reported by [46].

For a short-range ship application, using the same energy requirement and lifetime, authors in [30] concluded that the total cost of the supercapacitor storage system is 650 k€ with a volume of 5 m^3 and a total weight of 4000 kg in comparison to a 155.8 k€, 125.2 dm^3, 945 kg flywheel based energy storage system.

For a fuel economy application in a HEV, the results show that when cost and fuel economy were both considered, high speed flywheels were competitive with batteries and UC in [32].

Authors, in [45], stipulated that Li-Ion Capacitors (LIC) has the potential to supplement or replace mechanical flywheel for energy storage and pulsed energy in some high power applications. These LIC have three times the gravimetric energy density, and five times the volumetric energy density of standard electric double layer capacitors (EDLC). Nevertheless, the technology needs to achieve maturity and more development. High volume production will allow mass deployment of LIC in the energy storage market in the following years [47].

In [48], for 120 kW automotive application, the mass of the Maxwell Boostcap [33] UCs will be 370 kg (6.3 kJ/kg) in comparison to a 55 kg (30 kJ/kg) William Hybrid Power Flywheel (WHP MK4). Based on manufacturers' data, and for unequal power values, others comparison are performed between Maxwell Technologies state-of-the art BMOD0063 supercapacitors and other state-of-the art flywheels (GKN Hybrid Power and Flybrid Formula 1). In terms of mass, energy density and power density, the superiority is attributed to the flywheels in [15].

However, a significant difference between the capability of ultracapacitors and flywheels concerning the discharge pulse size and available energy is shown. The Flybrid, Ricardo and WHS flywheel systems specified have more available energy and provide a far higher pulse of power than the goals for the most demanding ultracapacitors (42 V Transient Power Assist) [49].

For electric vehicles, battery prices are already nearing the long sought goal of 100 $/kW h. In these applications, flywheels compete with ultracapacitors on the basis of the cost per unit energy delivered [44]. The energy cost has declined to 20,000 $/kW h. To the benefit of flywheels, motor drive power electronics costs have dropped dramatically approaching 5 $/kW [44]. On the other hand, the supercapacitor has a high acquisition cost [31]. According to Flybrid's cost estimates based on mainstream automotive market production volume, the standard flywheel should cost between $1000 and $3000 and the CVT should cost no more than $1500 which brings the total flywheel system cost to between $2500 and $4500 or $42–$75 per kilowatt [32]. The literature quotes ultracapacitors as costing between $13 and $51 per kilowatt [12].

Advanced flywheels have components that have been traditionally very expensive. However, key technologies are decreasing in price due to recent developments in other sectors. Power electronics are having their costs pushed down each year by the EV and power industries. Same reducing cost conclusions can be extended to ultracapacitors (Moore's law).

In the State of the Art (§ I.A) and in the present section, it has been listed references where flywheels and ultracapacitors are treated together in some electric transportation applications. In most cases, the comparison is based on an "apple to apple" analogy which means that the comparison analysis stands on manufacturers' data lists only. For this type of comparison, it is hard to find same specifications values in order to perform an accurate comparison (energy density, power density ...). This is essentially due to the lack of flywheel manufacturers in the market and to the short range of flywheels products selections. In some cases, this leads to excessive superiority conclusions of one energy storage on the other for a particular application.

In the present application, the flywheel and ultracapacitor are chosen as secondary energy storage implemented in the hybrid energy storage system of a two front-wheel drive vehicle. The ultracapacitor has been chosen according to precise specifications and requirements from a well-known manufacturers offering a large range of ultracapacitor products. In order to achieve adequate comparison, the flywheel and its driven motor has been designed in order to quote the defined requirements. In order to perform simulation, the two HESS obtained are then integrated in the overall model containing the vehicle and other major blocks (controllers, actuators ABS, TCS...). The comparison is carried out at two levels: The first level is the product level, based on similar specifications and requirements. The second level analyzes the secondary energy storage behavior in the system in the interest of investigating the main reasons of its use, which are to enhance the primary energy storage (battery) life and to respond to high dynamic power demand during extreme braking and start-up of the vehicle.

After reviewing comparison between FW and UC energy storage in literature, the next step is to explore the ultracapacitor solution, for the system described in § I.C, according to an appropriate sizing and selection criteria.

3. Ultracapacitors

3.1. Automotive applications

Ultracapacitors (Fig. 3) use electrostatic energy storage and electrochemical energy storage since the material separating electrodes is an electrolytic solution. Energy storage in the form of electrostatic potential is called the electric double layer capacitance (EDLC) [50]. One layer develops in the form of charge on the electrode while a second layer develops in the form of ions which diffuse from the electrolytic solution to the surface of the electrode [51]. UCs have almost quasi-infinite cycle life since there are no chemical reactions taking place.

PSA Peugeot-Citroën uses, in recent C4 and C5 models, Maxwell Boostcap 600 F/5V ultracapacitor storage device as booster in its micro-hybrid systems (e-HDI) [52]. Ultracapacitors are also used in Mazda-6 to enable regenerative braking on a 12 V Start/Stop micro-hybrid. Toyota, Honda and AFS Trinity have each developed concept/prototype vehicles to enable high performance through the use of ultracapacitors [51].

3.2. Ultracapacitor sizing

The ultracapacitor selection is mainly based on the maximal and minimal voltages of the ultracapacitor module, the nominal capacitance and the energy requirements. The minimal voltage operation is determined by the maximal current value of the DC/DC converter I_{c0max}. In general, it is chosen at 40% or 50% of the maximal voltage, such that

$$U_{c0min} \geqslant \frac{P_0}{I_{c0max}} \tag{5}$$

Fig. 3. BOOSTCAP BCAP0350 ultracapacitor from Maxwell®.

The maximal voltage of the ultra-capacitor should be less than the DC bus voltage and the DC/DC converter gain less or equal to 1. In terms of kinetic energy, the energy stored in the vehicle is:

$$E_{ke} = \frac{1}{2} m \times V^2 \tag{6}$$

This quantity has to be shared between the different energy converters and transformers, starting at the contact patch road/wheel arriving to the ultracapacitor, as shown in Fig. 4:

During braking, the fractions of energy to be shared among the wheels highly depend on the initial state of the vehicle, road surface type and condition, rotational speed of the motor... Other losses should be taken into consideration like the rolling resistance and the air drag resistance. These resistance forces contribute also to the vehicle deceleration. An approximate energy calculus should be done in order to carry out the ultracapacitor sizing.

The ratio between the friction force of the front wheel and the total friction force respecting the ECE R13 regulation [53] while assuring a maximal front/rear braking ratio is expressed by the coefficient

$$\beta_{hb-max} = \frac{2\sqrt{0.07 l_r h_g} + l_r + 0.07 h_g}{0.85 L}. \tag{7}$$

According to the vehicle dimension (Table 12), eighty-one percent of the total power should be recuperated by the front wheels and dispatched between electrical and mechanical brakes.

In worst cases, the efficiencies taken for the electrical/mechanical energy converters and transformers elements are considered equal to 90%. Another presumption also taken is that the third of the energy available at the front wheel would be recovered to electrical energy. For a vehicle speed of 80 km/h, the energy recovered by the UC and available at the front wheel is 81 kJ.

The total energy that could be recovered from an initial voltage U_{c0min} to the final voltage U_{c0max} is

$$\Delta E_{UC} = \frac{C_0}{2}(U_{c0max}^2 - U_{c0min}^2) \tag{8}$$

According to voltage and energy requirements, a series of 120 Mx BoostCap BCAP1200 P270 K04/5 ultra-capacitor cells [54] will be used in the studied application. Table 3 specifies the desired UC characteristics.

Table 3
UC characteristics.

Uc0max = 325 [V]
Uc0 min = 165 [V]
C0 = 10 [F]

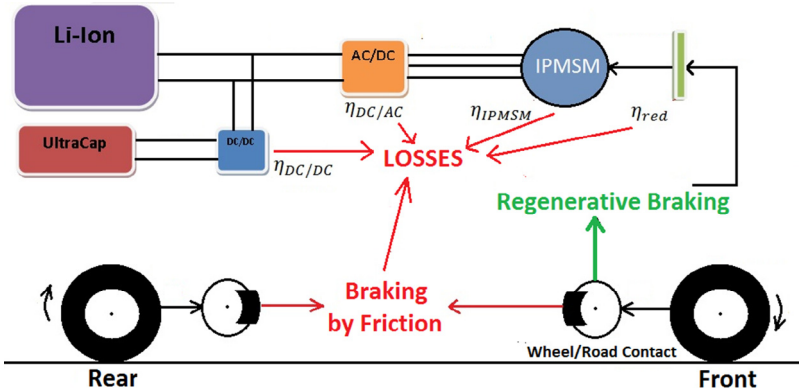

Fig. 4. Power Flow from Wheel/Road Contact to the Energy Storage Elements.

Table 4
UC cell characteristics [54].

Product name	BCAP1200 P270 K04/5
Rated capacitance (F)	1200
Rated voltage (V)	2.7
ESR (mΩ)	0.58
Leakage current (mA)	2.7
Absolute maximum Current (A)	930
Max continuous current (A) at 15C	70
Max continuous current (A) at 40C	110
Weight (g)	260
Stored energy (W h)	1.22
Emax (W h/kg)	4.7
Pmax (W/kg)	12,000
Terminal	Threaded/weldable
Length (mm)	74
Diameter (mm)	60.4

ΔE_c has a value of 392 kJ, which constitutes a full UC recovering for 4–5 braking operations according to the assumptions stated above. The UC characteristics are shown in Table 4.

The total mass of the ultracapacitors is 31.2 kg, with total volume of 25.443 dm^3. Extra spaces should definitely be taken into consideration ensuring support, cabling and electronic instrumentation for control and supervision.

The cost of the UC is estimated by using the graphic in [31]. The maximal energy that can be stored in the UC set is 146 W h. For a 33 $/W h, the total UC cost is approximated to 4818 $.

After ultracapacitor selection, the flywheel energy storage system design is described in the next section. The cost aspect is discussed. Interpretations and analyses of the obtained results for the selected ultracapacitor and FES are also highlighted.

4. Flywheels

4.1. Automotive applications

The application of the flywheel technology has lately resurfaced due to the endorsement made by the FIA, in October 2009, to the flywheel technology, stating that "Technology such as flywheels reducing dependence on batteries and concentrating on ICE load shift proves to be the most promising way forward".

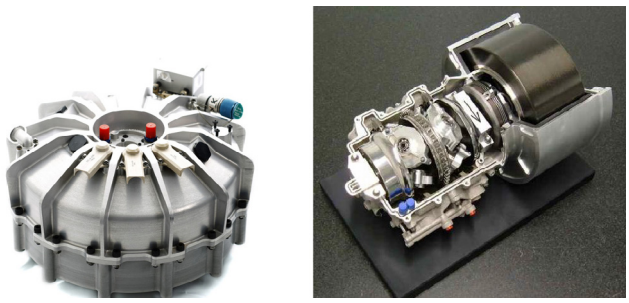

Fig. 5. At left, a WHP electrical flywheel. At right, a Flybrid mechanical flywheel.

This statement has been defended by the L-3MM flywheels systems in operation since 1988 on a total of 17 hybrid electric buses. Each of them has experienced 60,000 h of operation equivalent to 1,000,000 speed cycles.

The Porsche 911 GT3 R (Fig. 5) had a significant success in 2010 Nurburing Long Distance Championship using a William Hybrid Power (WHP) electrical flywheel powertrain. In June 2011, the Audi R18 E-Tron Quattro, equipped with a Flybrid flywheel mechanical powertrain flywheel system, was the first hybrid car to win Le Mans 24-h race [49].

In all above applications, flywheels are used to assist the ICE, considered as the prime mover. In the paper, the flywheel will be part of the HESS aiming to complement the battery protecting it from peak loads and enhancing its capacity and life cycle. Table 5 shows flywheel characteristics from different manufacturers.

For major literature references, the little information available concerning flywheels, for transportation applications, is mainly provided from manufacturers like Ricardo, WHP, Flybrid and L-3MM. Knowing that, flywheels technology, despite its history, is still a potential candidate energy storage for future mobility applications. So far, several prototypes have also been developed by Powerthru, Tribology System Inc., UTCEM and Flywheel Energy Systems Inc. [49].

For impartial comparison analysis with ultracapacitor storage, placed in a HESS and used as a secondary energy storage for battery enhancement life, a new flywheel has to be designed and comparison criteria should be established. The sizing of the two energy storage elements is based on the same energy and power capacities.

The modeling of the overall system is actually the integration of several blocks: the vehicle model has been developed using the dynamic and cinematic equations of a 5 DoF (degrees of freedom) vehicle (four rotation wheels and yawing movement), the driven motors and associated controllers, the braking control system, the traction control system, the hybrid energy storage system containing the energy storage element, the needed static converters and associated controllers. Each particular block of the overall system has been validated by authors in previous research papers [55–58]. The integration and the comparison analysis by simulation based on specific defined criteria of two different, custom designed, secondary energy storages during extreme braking and start-up operation of the EV constitutes the second objective of the present paper.

4.2. Flywheels design and sizing

4.2.1. Flywheel design

Regarding supercapacitors, manufacturers are well established in the market and offer a wide range of choices for supercapacitors products for a large variety of power range applications. For example, but not limited to, one can mention, for activated carbon ultracapacitors: Maxwell, Skeleton Technologies, Ness, EPCOS, Batscap, LS Cable, Power Sys; for hybrid ultracapacitors: JSR Micro, Yunasko; for propylene ultracapacitors: Panasonic, Asahi Glass (. . .) [20].

Table 5
Flywheel characteristics from different manufacturers.

Manufacturers	Type of the vehicle	Power (kW)	Mass (kg)	Driven	Rotation speed (rpm)
WHP	Porsche 911 GT3 R	120	57	Front Axle (60 kW each)	40,000
WHP	Porsche 918 RSR	150	27	Front axle (75 kW)	
Flybrid	Audi R18 E-Tron Quattro	97	17.2	Clutched flywheel Transmission (CFT)	
Flybrid	Jaguar XF	60	64.9	Clutched Variable Transmission (CVT)	60,000
Flybrid	Volvo	60	60	Rear axle	60,000

As for flywheel energy systems, the choice is much more limited to a small number of manufacturers and to a much narrower power range applications. More concerns should then be dedicated to the flywheel design and sizing applied to the particular application relative to the present research paper.

The shape used is the dominating shape in flywheels which is the hollow cylinder. This geometry was chosen due to its simpler manufacture and lower cost, when compared to other geometries. The energy stored in a flywheel is:

$$E = \frac{1}{4}\pi h\rho(r_o^4 - r_i^4)\omega^2 \tag{9}$$

where r_o the outer radius, r_i the inner radius, h the length of the flywheel cylinder, ρ the rotor material density, ω the angular rotating speed.

Materials composing the wheel has a limited rotating speed due to the stress developed, called tensile strength, σ, composed of two kinds of forces: the radial stress σ_r and the tangential stress σ_t (known as hoop stress).

In general, the outer and the inner radius, the stress forces relationships are required to dimension the wheel:

$$\begin{cases} \frac{\sigma_r(r)}{\rho\omega^2 r_o^2} = \frac{3+\upsilon}{8}\left(1 + \frac{r_i^2}{r_o^2} - \frac{r_i^2}{r^2} - \frac{r^2}{r_o^2}\right) \\ \frac{\sigma_t(r)}{\rho\omega^2 r_o^2} = \frac{3+\upsilon}{8}\left(1 + \frac{r_i^2}{r_o^2} + \frac{r_i^2}{r^2} - \frac{1+3\upsilon}{3+\upsilon}\frac{r^2}{r_o^2}\right) \end{cases} \tag{10}$$

where υ is the Poisson ratio depending on the material of the rotor. Results show that the tangential stress is always more important than the radial stress [59]. The maximum of the tangential stress is given by:

$$\frac{\sigma_t}{\rho\omega^2 r_0^2} \cong 1 \tag{11}$$

Using the above approximation in the energy equation Eq. (9), the energy limit achieved:

$$E_{lim} = \frac{1}{4}\pi h\sigma_t\left(1 - \left(\frac{r_i}{r_o}\right)^4\right)r_o^2 \tag{12}$$

The best relationship between r_i and r_o is to weight equally the energy limit per total volume (J/m^3) and the energy limit per total volume of rotating mass, giving then

$$\frac{r_i}{r_o} = \frac{\sqrt{2}}{2} \tag{13}$$

For size limitation, $h = 2r_o$ will be chosen, having then

$$E_{lim} = \frac{3}{8}\pi r_o^3\sigma_t \tag{14}$$

4.2.2. Flywheel rotor's geometry and materials

The speed is limited by the tensile strength developed in the wheel. More general expressions for the maximum energy density, valid for all flywheel shapes can be written as:

$$e_v = K \cdot \sigma \tag{15}$$

$$e_m = \frac{K \cdot \sigma}{\rho} \tag{16}$$

where e_v is the kinetic energy per volume, e_m the kinetic energy per unit mass, K the shape factor (<1), σ the maximum stress in the flywheel, ρ the mass density. For a hollow cylinder, K is equal to 0.5.

The equations Eqs. (15) and (16) above show that materials, with low density and high tensile strength, are excellent for storing kinetic energy. Table 6 lists characteristics of materials used in flywheel rotors. It shows that steel has lowest energy density (and price), followed by fiber glass and then composite carbon materials.

The flywheel maximum speed (respectively minimum speed) is 27,500 rpm (respectively 10,000 rpm). According to equations design described above and using Table 6, the flywheel dimensions, for different materials, are presented in Table 7:

The inertia value is 0.1104 kg m^2. The total energy capacity that can be stored is 0.127 kW h or 458 kJ. Avoiding mechanical stress on the flywheel, the speed varies between 27.5 krpm and 10 krpm ensuring a 397 kJ energy per cycle, which is 86% of the total stored energy. Considering cost and volume, the AlSi 4340 material is an optimized solution in terms of inertia value and rotational speed range for the application. For the inertia value of 0.1104 kg m^2, other materials (fiber glass and composite carbon) have higher volume and cost, but a lower mass. On the other hand, these materials can surpass the defined maximal speed by far and have a higher security value. The security factors can be measured by the value of the maximal speed allowed and also the ratio between the min-

Table 6
Characteristics of materials used in flywheel rotors [60,31].

Materials	Density (kg/m^3)	Tensile strength (MPa)	Maximum energy density (W h/kg)	Cost ($/kg)
AlSi 4340	7700	1520	27	1
36NiCrMo16	7800	880	15	6.6
Maraging 300	7800	1850	32.9	36
E-Glass	1900	1350	98	26
S2-Glass	1920	1470	106	25
Kevlar Epoxy	1370	1400	141	79
Carbon T1000	1520	1950	178	102
Carbon AS4C	1510	1650	150	31

Table 7
Dimensions, mass and cost of the flywheel depending on rotor material.

Materials	r_o (m)	r_i (m)	h (m)	Volume (m^3)	Mass (kg)	Material cost ($)
AlSi 4340	0.090555	0.064032	0.18111	0.004666	17.96292	17.96292
36NiCrMo16	0.090322	0.063867	0.180643	0.00463	18.05588	119.1688
Maraging 300	0.090322	0.063867	0.180643	0.00463	18.05588	647.4837
E-Glass	0.119801	0.084712	0.239602	0.010803	10.26319	265.3033
S2-Glass	0.11955	0.084535	0.2391	0.010736	10.30626	253.5341
Kevlar Epoxy	0.127899	0.090438	0.255797	0.013146	9.004694	713.1718
Carbon T1000	0.125268	0.088578	0.250537	0.012351	9.386813	955.5776
Carbon AS4C	0.125434	0.088695	0.250868	0.0124	9.362062	293.0325

Table 8
Rotor material security factor.

Materials	N_{max} (rpm)	Security factor ratio
AlSi 4340	33,129	1.6
36NiCrMo16	25,110	0.95
Maraging 300	36,408	2
E-Glass	47,510	3.4
S2-Glass	49,421	3.7
Kevlar Epoxy	53,369	4.3
Carbon T1000	61,053	5.65
Carbon AS4C	56,272	4.8

imal tensile strength and the tensile strength of the material (taken as half of the actual tensile strength for safety issue).

The maximal speed is calculated by:

$$N_{max} = \frac{30}{\pi}\sqrt{\frac{\sigma_t}{\rho r_0^2}} \tag{17}$$

The minimal tensile strength is measured by:

$$\sigma_{tmin} = \rho\omega_B^2 r_0^2 \tag{18}$$

The security factors for different rotor materials can be found in Table 8:

It is shown that carbon composite materials offer better security measures for high speed flywheel applications. The steel material has the lowest security factor. The AlSi 4340 appears as a good and economic candidate regarding maximal rotational speed and security factor ratio.

4.2.3. Electrical machine sizing

For the electrical machine dimension, the equation relating the machine dimensions with its power rating is used:

$$D^2 \cdot L_m \cdot N = \frac{5480}{A \cdot B_{gav} \cdot K_w \cdot \cos\varphi \cdot \eta} \cdot P_{kW} \tag{19}$$

where K_w is the winding factor, A the specific electric loading, B_{gav} the specific magnetic loading, L_m the length of the machine, η the efficiency, $\cos\varphi$ the power factor, P_{kW} the output power, D the diameter and N the machine rotational speed.

The nominal value of A is between 15,000 A/m and 35,000 A/m. B_{gav} is usually 0.35–0.6 Wb/m^2 for 60 Hz machines. K_w, winding factor, is function of the values of slots per pole per phase. For the machine design example, a winding factor of $K_w = 0.966$ will be used, which corresponds to a 2 slots per pole per phase machine.

For an aspect ratio of 4, the inner diameter of the machine can be written as:

$$D_{in}^3 = \frac{5480}{A \cdot B_{gav} \cdot K_w \cdot \cos\varphi \cdot \eta \cdot N \cdot \pi} \cdot P_{kW} \tag{20}$$

Table 9
Flywheel motor dimensions.

D_{in}	8.6 cm
D_{out}	15.56 cm
L_m	26.9 cm

The length is given by the equation:

$$L_m = \pi \cdot D_{in} \tag{21}$$

According to [61], relation between D_{out} and D_{in}, for a two poles machines:

$$\frac{D_{in}}{D_{out}} = 0.55 \tag{22}$$

Applying the above equation, Table 9 shows the flywheel permanent magnet synchronous motor dimensions.

The total volume of the FW and motor set is 10 dm^3. Extra spaces should be added for the containments, cooling system and electronic control and supervision instrumentation.

In order to evaluate the total mass of the electrical machine, the volume of the stator core, the total windings and the rotor should be calculated.

The conductors in series per phase is given by:

$$N_c = \frac{E_v}{2.22 f K_w \Phi_p} \tag{23}$$

where Φ_p is the flux per pole:

$$\Phi_p = B_{gav}\frac{\pi D L_m}{p} \tag{24}$$

Table 10 shows the mass and the cost of each part of the electrical machine.

The total cost is to be multiplied by the manufacturer factor cost of development and manufacturing, based on manufacturer's data. If the factor cost is equal to 7, then the total cost of the machine is 3323 $. Using the same factor cost for the FW construction, the total cost set (FW + motor) will be 3500 $. Whereas, the total mass of the system is 58 kg.

4.2.4. Interpretation and synthesis

According to the obtained results, Table 11 summarizes the major characteristics of the secondary energy storage systems to be used in the application. The term Flywheel Energy System (FES) is used to include electrical machine. The total energy is the maximal energy stored in the UC or the FES. This energy is not totally exploited by the HESS, due to the minimal voltage value of the UC or the minimal speed of the FES. As explained, the

Table 11
Techno-economic optimization for the UC and the FES solutions.

	UC	FES
Power (kW)	60	60
Energy (Wh)	146	127
Energy (kJ)	528	458
Volume (l)	25.44	10
Mass (kg)	31.2	58
Total cost ($)	4818	3500
Specific energy (W h/kg)	4.7	2.2
Energy density (W h/l)	5.7	12.7
Specific power (kW/kg)	1.9	1
Power density (kW/l)	2.4	6
Cost per unit power capacity ($/kW)	80.3	58.3
Cost per unit energy capacity ($/kW h)	33,000	27,560

Table 10
Mass and cost of electrical machine materials.

Materials	Density (kg/m^3)	Volume (m^3)	Mass (kg)	Material cost ($/kg)	Total material cost ($)
Copper	8960	0.0013	11.5	6.6	76
Iron	7850	0.0034	26.7	3.3	88
Neodymium magnet	7500	0.00026	2	154	310
Total			40 kg		474 $

amount of energy for a complete charge/discharge cycle is 400 kJ (Ref. § III.B).

The results show that for equal values of power, equal values of energy (400 kJ), and depending on the design methods detailed above, the designed FES is more favorable than UC in terms of volume, energy density, power density and even cost ($/kW and $/kW h). As a reminder, the rotor flywheel material chosen (AlSi 4340) was the heaviest but the cheapest among the used rotor materials listed in Table 6. This material was chosen according to specific optimization criteria. In fact, if another material was selected, like the carbon AS4C for example, the conclusions remains the same, except for the cost of the system. However, the use of UC is encouraged if weight, specific energy and specific power are major selection criteria.

As for the cost issue, the UC set has been approximated at 4 818 $ (USD) (Ref. § III.B) whereas the flywheel system designed (including the electrical motor) has been evaluated at 3 500 $ (USD) (Ref. § IV.B.3). This enforces the high acquisition cost assumption for the ultracapacitor revealed in Section 2.3.

In order to increase the recovered energy, exceeding the UC maximal voltage would definitely damage the UC. In fact, beyond the maximum charging voltage, UC faces electrochemical instability, leading directly to a capacity fade and a life reduction of the storage element. The dynamic voltage equalization for the series connected ultracapacitors will also be highly affected. Whereas, for the FW, the increase of the speed is limited by the tensile material strength of the rotor and by the electromagnetic and mechanical constraints of the motor as well as its control performance. According to Table 8, an overspeed of 5.5 krpm above the maximal speed of 27.5 krpm is still permissible for the chosen FW material. The power electronic based converters for FES (inverter) or UC (3-level DC/DC converter) were not taken into consideration in the cost comparison process. It has been supposed that their prices are similar.

In this section, flywheel energy storage design and specific comparison with the ultracapacitor have been treated. These storage elements are being incorporated in the vehicle system described in the next section.

5. System presentation

5.1. Vehicle modeling

The vehicle simulator was developed by the author to allow for novel simulations of EV analyzing energy and power transfer, transient physical values reading (electric/mechanic/kinematic/dynamic) and the vehicle behavior. This method of simulation helps to incorporate and to integrate different types of energy storage elements as well as different control methods for actuators and power electronics devices. The model could also compute several internal physical quantities and coefficients of the vehicle such as normal forces, lateral/longitudinal friction forces, yaw/lateral/longitudinal acceleration/speed/displacement, lateral/longitudinal/resultant slip and friction coefficients (...).

5.2. Hybrid Energy Storage System (HESS)

The considered EV is driven by two 30 kW interior permanent magnet synchronous motors (IPMSM). The first HESS already developed by authors in [55,56] (Fig. 6) contains a Li-Ion battery and an ultracapacitor (UC) storage elements sources as well as a dissipative resistor. The UC will be involved, mainly, in braking and traction modes. The role of the resistor is to protect the DC bus and the battery according to the voltage and current constraints while braking.

The second HESS contains a Li-Ion battery and a FES as a secondary storage elements as shown in Fig. 7. The control of the electrical motor of the FES is described in [57].

The objective is to reduce the use of the battery during extreme power demand. The secondary storage element should absorb or deliver the needed power as much as its physical characteristics are not exceeded. For this purpose and in the care of doing a fair comparative study, the control strategy for both HESS is the same. It is based on the secondary storage element intervention in order to eliminate battery interference, if possible, even if it requires its maximal power solicitation. For example, in braking mode, the energy recovery is taken in priority by the secondary storage elements as long as these elements can support this recovery.

5.3. Braking and traction control systems

5.3.1. Braking control system

In the paper, the regenerative braking is prioritized to the friction braking as long as the system conditions and safety constraints permit. The braking control mode is based on the inequality rules cited in the international Braking Regulation of the Economic Commission for Europe of the United Nations Organization No. 13 Harmonized (UN/ECE R13H) for Road Vehicles of category M1 (vehicles used for the carriage of passengers and comprising not more than eight seats in addition to the driver's seat), [62,63]. An anti-lock braking system (ABS) is being integrated. The constrained braking regenerative control method is developed by authors in [58]. The braking forces distribution (front/rear, mechanical/electrical) and evaluation depends on the road surface condition and type ensuring stability, maneuverability, and avoiding wheels locking. Fig. 8 shows the inputs and outputs of each model and control block involved in the braking operation.

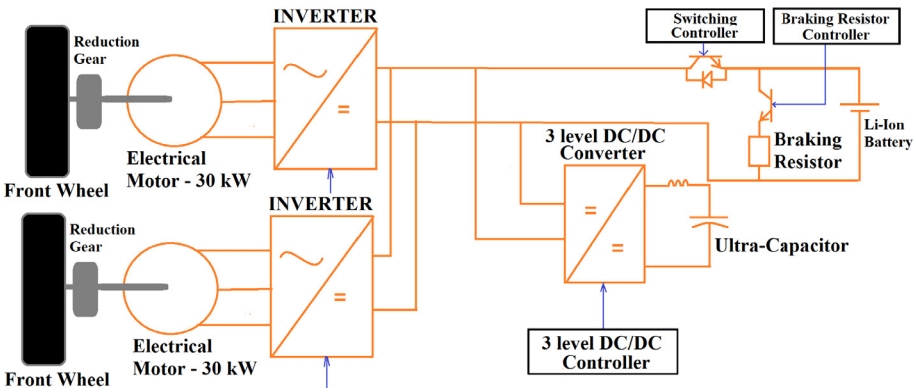

Fig. 6. HESS involving an UC as a secondary energy storage element.

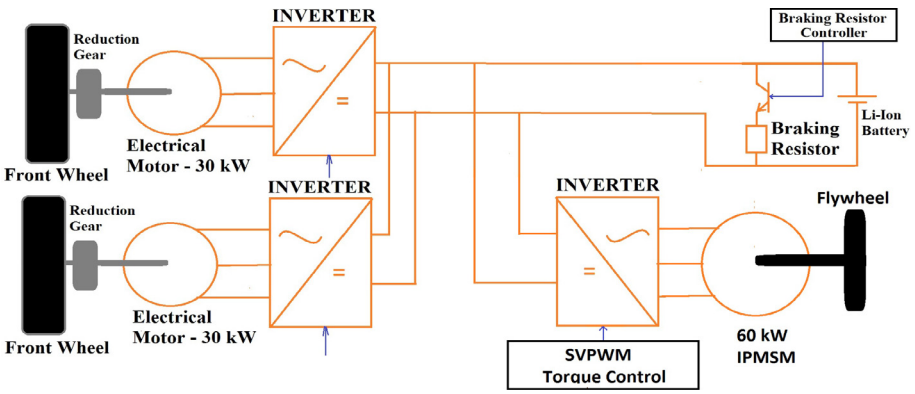

Fig. 7. HESS involving a FES as a secondary energy storage element.

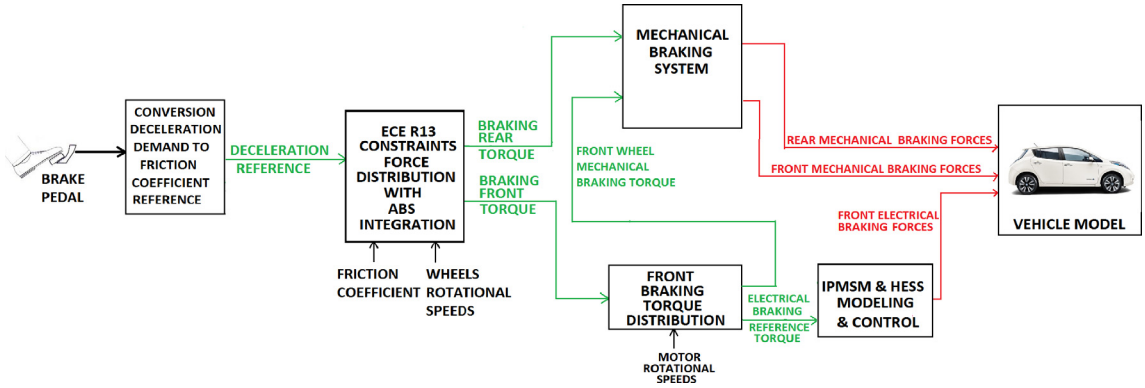

Fig. 8. Model and control blocks of the braking simulation system.

5.3.2. Traction control system

The traction control system is based on a sliding mode control of the slip coefficient of the wheels. For different road surface type and condition, the friction coefficient vs the slip coefficient according to Burckhardt model [64] is plotted in Fig. 9.

In order to impose a maximal friction force on the wheel, on a certain road type, it will be convenient to ensure the maximal friction coefficient μ_{max} by regulating the slip coefficient at the value λ_{max}.

The slip ratio can be represented as:

$$\lambda_i = \frac{\omega_i \cdot r - v_{wi}}{\omega_i \cdot r} \tag{25}$$

where λ_i is the slip coefficient of the wheel i (r for right and l for left), v_{wi} the speed of the wheel i and ω_i for the wheel rotational speed of the wheel i.

The slip controller will be designed according to the sliding mode controller described in [65,66]. A sliding mode slip control is known to be robust to changing and unknown road condition (compared to a simple wheel acceleration control). A sliding surface s should be designed in order to be forced to zero in spite of disturbances and parameters uncertainties. In order to prevent a simple bang-bang control acting on the sign of the error and to ensure an exponential error convergence dynamics, the sliding surface is chosen as a weighted sum of the state (slip coefficient) error and the integrated state error. The control system will then force the system onto the sliding surface, and the trajectories will slide along $s = 0$ with the dynamics determined by the definition of the sliding surface. Uncertainties are taken on the vehicle mass, the wheel radius, the rolling resistance coefficient and the aerodynamic drag wind resistance coefficient. The road surface types are considered to be known and no friction coefficient estimation should be implemented in the model. The output of the controller is the reference torque to be applied to the HESS according to the diagram in Fig. 10.

After describing the model system, simulations are performed in the next section for extreme braking and start-up operations of the vehicle and for different road types and conditions.

6. Simulation validation

6.1. Introduction

The main purpose of the present research work is to reduce the battery stresses during high current demand. The life and state of the battery are outstripped by any other constraint, such as the recovery power rate, for example. The high power demand is generated in two cases. In braking mode, for a vehicle running at a high velocity, the driver requires an urge and immediate stop. Or in traction mode, the vehicle is initially at rest, the driver presses on the pedal for an immediate and brutal acceleration.

The system behavior regarding traffic condition variation is quiet interesting. Nevertheless, it should require ultrafast and high memory computers. In fact, the developed Simulink blocks (vehicle, driven motors, converters and associated controllers) are modeled starting from their primitive state equations. This choice has been taken in order to analyze and study other fields such as the effect of the braking method [58] or the control of the HESS [55,57]. This makes each simulation test a memory and time consuming operation.

Though, during dense city traffic variation, the extreme braking and start-up operations have low statistical occurrence. In that case, the battery power solicitation could not present a great concern for its life.

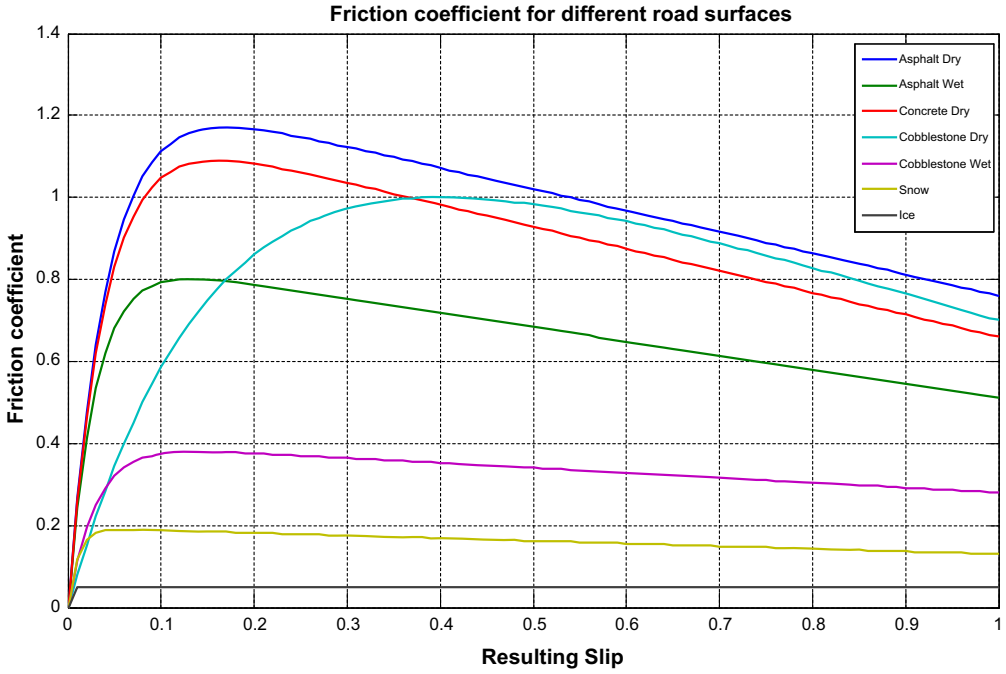

Fig. 9. Friction Coefficient for Different Road Surfaces.

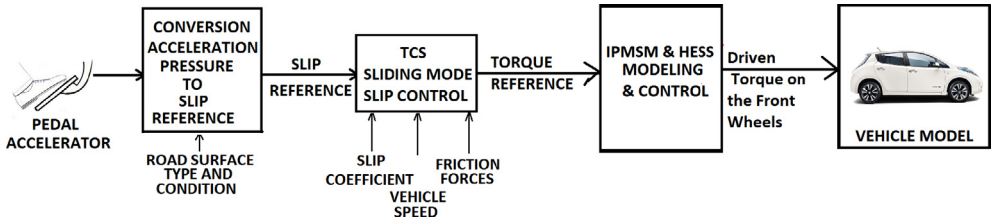

Fig. 10. Model Blocks for the TCS.

The traction control used is based on a sliding mode slip control known for its robustness according to disturbances, model and parameters uncertainties. Uncertainties are taken on the vehicle mass, the wheel radius, the rolling resistance coefficient and the aerodynamic drag wind resistance coefficient.

The software simulation tool is Matlab/Simulink®. At the beginning of the simulation, a Matlab program script will be launched in order to define the mandatory elements of the system: (1) the vehicle parameters, the external dynamic and the road type parameters, (2) the vehicle driving motors parameters, limiting operation points and regulators gains, (3) the HESS characteristic parameters and the corresponding regulators gains of the different power electronics based converters (AC/DC for FW application or DC/DC for UC application), (4) the flywheel motor parameters, limiting operation points and regulators gains. For each test, after defining the initial system state (initial vehicle velocity, initial flywheel speed, initial UC voltage, road surface type...) and generating all the above quantities, a Simulink program will be launched. At the end of the simulation, a Matlab program script plots the corresponding figures and delivers the characteristic values of the overall system.

The vehicle model dimensions are based on a Nissan Leaf® EV (Table 12).

Table 12
Vehicle model parameters based on Nissan Leaf®.

Parameters	Description	Value
$m[kg]$	Gross vehicle mass	1890
$L[m]$	Vehicle wheel base	2.7
$l_r[m]$	Distance from the rear wheel axle to the center of mass	1.4
$l_f[m]$	Distance from the front wheel axle to the center of mass	1.3
$h_g[m]$	Distance from the center of mass to the ground	0.5
$r[m]$	Wheels radius	0.3

6.2. Tests definition

The tests are performed for two types of road surface types and conditions. The first road is a high friction road specified as a good condition dry asphalt road. The maximal friction coefficient μ_{max} of this type of road is 1.17 obtained for a slip coefficient λ_{max} of 0.17 (Fig. 9). The second road is a low friction road specified as a good condition wet cobblestone road. This type of road has a maximal friction coefficient μ_{max} of 0.38 obtained for a slip coefficient λ_{max} of 0.14. The tests are performed for an extreme braking operation as defined in §V.C.1 and for a sliding mode traction control operation as described in §V.C.2. Power plots for some distinctive tests will be shown and the recovered/delivered energy quantities for each element are presented in tables. Tests are performed according to initial state of energy (SOE) of the secondary energy element of the HESS defined by:

$$SOE_{FW} = \frac{1}{2} J_{FW} \frac{(\omega_{FW}^2 - \omega_{FWmin}^2)}{E_{FW}} \tag{26}$$

$$SOE_{UC} = \frac{1}{2} C_0 \frac{(U_{c0}^2 - U_{c0min}^2)}{E_{UC}} \tag{27}$$

where SOE_{FW} (respectively SOE_{UC}) is the state of energy of the FW (respectively the UC), E_{FW} (respectively E_{UC}) is the energy capacity of the FES (respectively the UC).

The braking control system will operate at extreme braking conditions, known also as hard or sudden braking. Which means that the braking forces would be quantified and distributed according to the type of road in order to prevent locking of wheels and to ensure the minimal possible stopping time. The braking tests were done on the vehicle model of Table 12. The initial velocity of the vehicle was considered to be 80 km/h. The tests were performed on two different types of road: a good condition asphalt dry road and a good condition cobblestone wet road; and for different SOE of the secondary energy element. The SOE was chosen to be respectively 10%, 25%, 50%, 75% and 90% corresponding to a rotation speed of 10,000 rpm, 16,250 rpm, 20,691 rpm, 24,334 rpm and 26,280 rpm for the FW, and to a voltage of 165 V, 216.4 V, 257.7 V, 293.3 V and 312.7 V for the UC. In each test, the interference of the battery and the severity of this interference in terms of current and energy absorbed by the battery are indicated. The presence of the braking resistor is to protect the battery from overcurrent and excessive overvoltage using a pseudo-cascade controller [67]. In order to prevent a high in-rush current during regenerative braking, the battery current is regulated to a reference current value (1C rate) which is equal to the nominal battery capacity of 66.2 A h. Charging the battery with higher rate current would definitely compromise the battery life and lead to its degradation (cf. § I.B).

6.3. Braking tests

6.3.1. High friction road type

The following tables show the energy recovered by the primary (Li-Ion battery) and the secondary (FES or UC) storage elements as well as the energy dissipated by the braking resistor. For the first test, the asphalt dry road type is taken. In this case, the braking time is 2.26 s, the traveled distance is 26 m. The results are shown in Table 13 for the FES as secondary energy storage element, and in Table 14 for the UC.

In the FES case, and for lower rate SOE, the power could not be totally handled by the FES so the battery interference is inevitable. In fact, the FES power is limited by the rotational speed and the maximal FES torque (§ II.A). At higher rotational speed, the energy recovered by the battery is less because the power that could be absorbed by the FES is greater. Whereas, for the UC, and for the reasons explained in (§ II.A), the UC is capable of absorbing the total power as long as the SOC of the UC does not reach 95%. This security factor is not taken into consideration for the FES case because as shown in Table 8, the maximal rotational speed is within the acceptable speed range.

For a SOE of 50%, Fig. 11 shows the power of the different electrical actuators (two driving motors), the storage elements (battery and flywheel) and the braking resistor. The figure illustrates also the increasing power strength of the FW as it gains speed (between 0 and 1 s). After 0.86 s, the FES is capable of absorbing the total energy coming from the motors. It is noted that the electrical power of the driving motors decreases as long with the vehicle speed.

The flywheel speed and torque are shown in Fig. 12. At the beginning of the simulation, the flywheel torque is regulated to its maximal value of 22 N m. The power capability of the flywheel power is increasing along with its speed. At t = 0.86 s, the flywheel torque begins to decrease in order to quote to the braking power required by the braking system. At the end of the braking, the flywheel speed reaches 21,940 rpm.

Whereas for the same value of SOE, the UC measurements are shown in Fig. 13. The current is regulated in order to recover the totality of the power, as designed. At t = 0.4 s, the power is at its maximal value of 61.2 kW. The UC voltage and state of charge increase along the charging of the UC. During this test, the battery didn't recuperate any power.

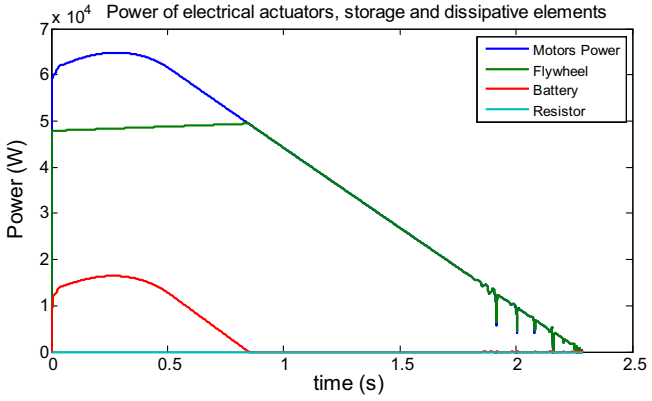

Fig. 11. Power of electrical elements for a regenerative braking test on an asphalt dry road type and for a SOE of 50% for the FES.

Table 13
Regenerative braking on an asphalt dry road - FES as secondary energy storage.

SOE (%)	Energy recovered/dissipated (kJ)			Battery intervention time	Battery current	
	Flywheel	Battery	Resistor		Peak	Current controller activated
0	47.28	31.35	0.2	Until 1.53 s	99.3 A	√
25	66.5	19.55	0.0018	Until 1.13 s	69.7 A	√
50	76.66	9.8	0	Until 0.86 s	44 A	X
75	82.85	3.67	0	Until 0.63 s	21.6 A	X
90	85.2	1.3	0	Until 0.5 s	10.4 A	X

Table 14
Regenerative braking on an asphalt dry road - UC as secondary energy storage.

SOE (%)	Energy recovered/dissipated (kJ)			Battery intervention time	Battery current	
	UC	Battery	Resistor		Peak	Current controller activated
0	81.8	0	0	X	X	X
25	83.16	0	0	X	X	X
50	83.9	0	0	X	X	X
75	65.38	18.14	1.26	Starting at 1.25 s	94.78 A	√
90	0.08	53	33.36	All the time	165 A	√

For higher SOE rate, the FES is advantageous on the UC. In fact, once the UC is full of charge, the battery (and the braking resistor) should absorb the totality of the braking energy. Whereas, for the FES, a greater speed allows a greater power and thus less battery interference. As example, an SOE of 75% is taken in order to perform the comparison. Fig. 14 shows the current absorbed by the battery in the FES and UC cases. In the case of the UC, the battery handles a current of 94.78 A for 100 ms, after that pseudo-cascade controller enters in operation to regulate the current to 66.2 A.

Fig. 15 shows the current of the UC. The current is brutally downed to zero when the SoC reaches 95%. The battery found itself constrained to handle full current the first 100 ms before the intervention of the braking resistor.

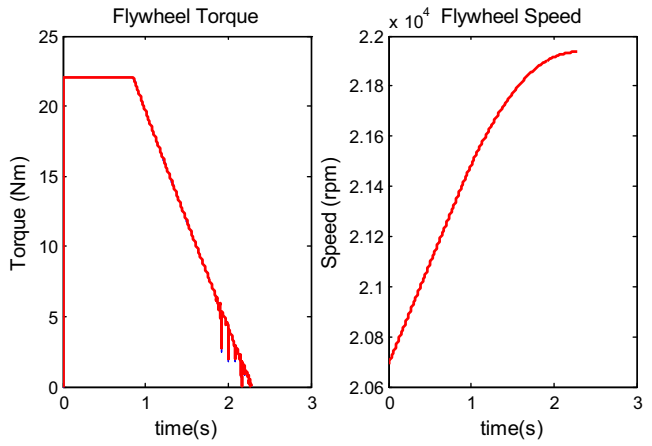

Fig. 12. Flywheel torque and speed for a regenerative braking test on an asphalt dry road type and for a SOE of 50% for the FES.

6.3.2. Low friction road type

For the second braking test, the cobblestone wet road type is taken. In this case, the braking time is 6.973 s, and the traveled distance is 76.6 m. The results are shown in Table 15 for the FES as secondary energy storage element, and in Table 16 for the UC.

Same conclusions as the high friction road can be brought for the low friction road. However, it is important to notice that in that type of road, the energy quantity available to be recovered is greater than the high friction road, because the power involved in the braking process is lower. The energy storage elements should take advantage and recover more energy. In fact, the recovering of the kinetic energy value (of 483 kJ), the same for all types of road, has to be prolonged for a much longer braking time. Knowing that, even if the overall braking power is lowered by the braking control

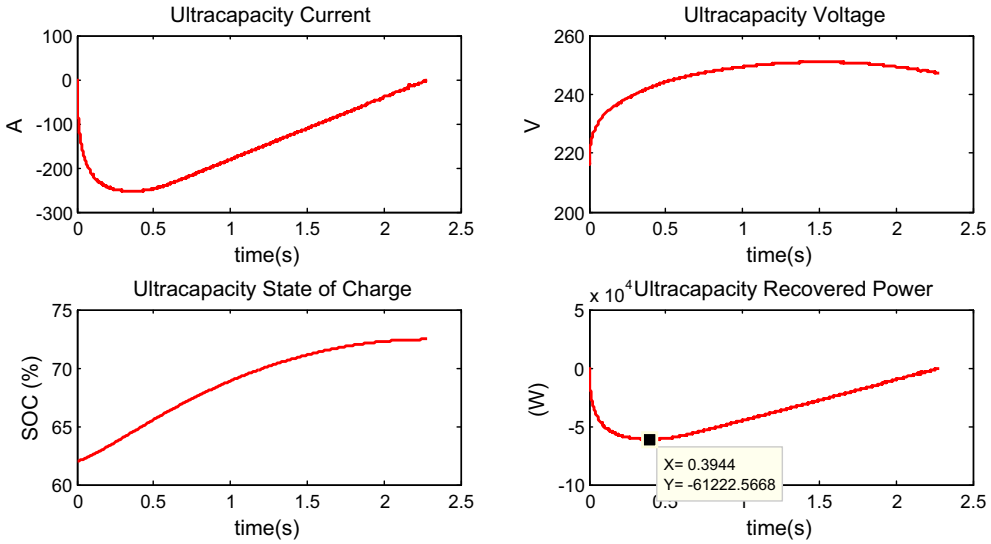

Fig. 13. Ultracapacitor measurements for a regenerative braking test on an asphalt dry road type and for a SOE of 50%.

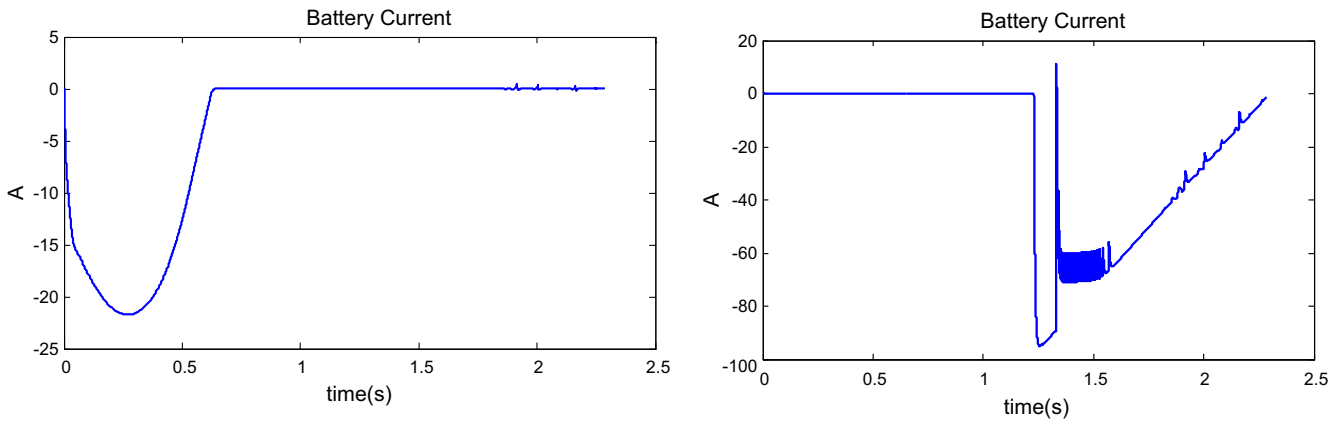

Fig. 14. Battery current for the FES case (at left) for the UC case (at right) - SOE = 75%.

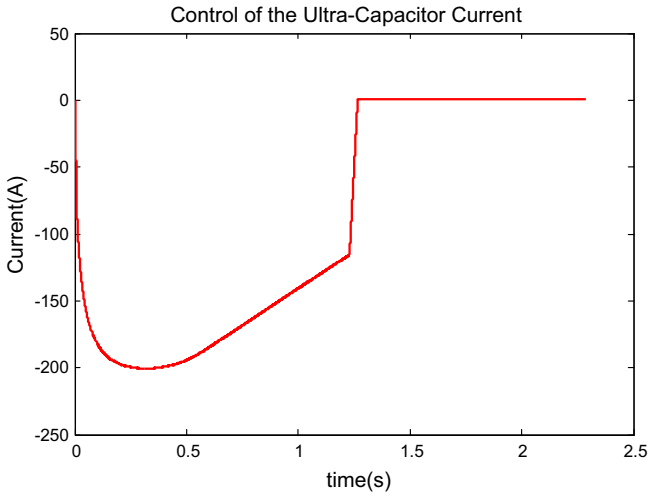

Fig. 15. UC current for a regenerative braking test on an asphalt dry road type and for a SOE of 75% for the FES.

system, the electrical actuators (driving motors) as well as the storage elements are operated at higher power capabilities. In fact for SOE = 90% and FES solution, the battery current controller is being activated for this type of road and the battery has to support a current of 95.2 A, while it isn't the case for high friction road.

Fig. 16 shows the current plots for a SOE of 90% of the FES and the UC. Same conclusions can be brought. The FES has handled the total regenerative power until 2 s of braking, after attaining its maximal speed of 27,500 rpm, it handovers the power recovery to the battery. The stress on the battery is higher on the UC in that particular case. Whereas, for lower SOE rate (SOE = 0%), the UC is able to recover all the power needed. The FES gains power recovery while increasing its speed.

If the energy management system requires the discharging of the secondary energy storage throughout the driving in order to recover the braking energy, the use of UC is more advantageous than the use of a FES in all cases.

6.3.3. Traction tests

The traction tests are performed for the vehicle, initially at rest, on the two types of road. The start-up of the vehicle is performed at its maximal traction capabilities controlled by the TCS system according to the road type. The acceleration time is for 6 s. The SOE was chosen to be 100%, 75%, 50%, 25% and 10% corresponding to a rotation speed of 27,500 rpm, 24,334 rpm, 20,691 rpm, 16,250 rpm, and 12,870 rpm for the flywheel, and to a voltage of 325 V, 293.3 V, 257.7 V, 216.4 V and 187.2 V for the UC.

Table 15
Regenerative braking on a cobblestone wet road - FES as secondary energy storage.

SOE (%)	Energy recovered/dissipated (kJ)			Battery intervention time	Battery current	
	Flywheel	Battery	Resistor		Peak	Current controller activated
0	134.2	45.1	0.06	Until 3 s	98 A	√
25	166	17.8	0.0001	Until 1.5 s	72A	√
50	178.5	3.54	0	Until 1 s	44.15 A	X
75	183.13	0.8	0	Until 0.3 s	22.2	X
90	94.7	81.8	0.1	Starting from 2.01 s	95.2 A	√

Table 16
Regenerative braking on a cobblestone wet road - UC as secondary energy storage.

SOE (%)	Energy recovered/dissipated (kJ)			Battery intervention time	Battery current	
	UC	Battery	Resistor		Peak	Current controller activated
0	176.8	0.2	0	X	X	X
25	176.8	0.2	0	X	X	X
50	179.7	0.2	0	X	X	X
75	64.95	101	16	Starting at 1.28 s	115.5 A	√
90	0.112	137	46.52	All the time	165 A	√

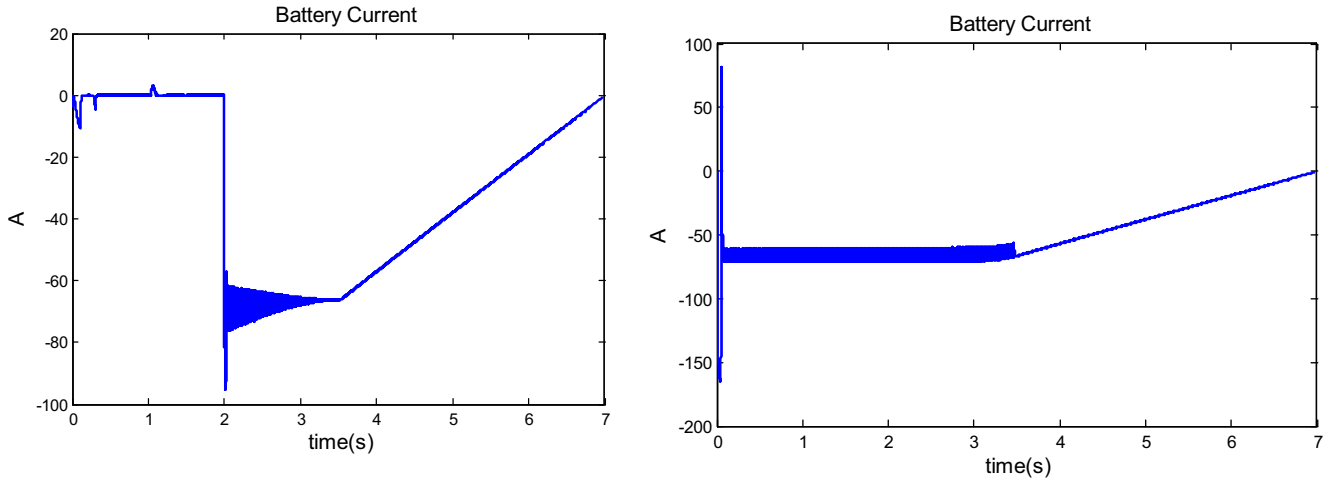

Fig. 16. Battery current for the FES case (at left) for the UC case (at right) - SOE = 90%.

In traction mode, the vehicle behavior is determined, only, by the power of the driving motors limited to 60 kW, which is not the case in the braking mode. In the braking mode, the mechanical friction braking system handles the greater part of the braking power. The vehicle being at a higher velocity, the driving motors rotate also at higher speed. Once the braking operation is started, the motors are capable of generating electrical power at higher rate. This isn't the case in start-up mode. The vehicle being at rest, the mechanical power generated by the motors goes from zero. The acceleration rate is limited to the maximal torque generated by the driving motors. The TCS chosen delivers the reference torque to the motors controller. Obviously, in that particular system, the reference torque is much higher than the maximal motor torque, which leads to a similar behavior of the HESS system for the two types of road. In high friction road type, in 6 s, the vehicle travels 26.3 m and the attained speed is 31.4 km/h. In low friction road type, the vehicle travels 30.3 m, and the attained speed is 36.2 km/h.

For high friction road type, Tables 17 and 18 show the delivered energy and battery interference for the two types of HESS. For low friction road type, Tables 19 and 20 show the delivered energy and battery interference for the two types of HESS.

For higher SOE (100–50%), the flywheel and the UC are capable of delivering the totality of the energy. The battery is not solicited in all the 6 s during vehicle start-up. The behavior of the two HESS solutions is the same for the two types of roads. And no stresses are exerted on the battery.

At lower SOE, for example SOE = 25%, the battery interferes after 5 s of starting-up, but the current delivered is different for both solutions. For example, for an SOE of 25%, cobblestone wet road, the constraints on the battery for a FES case is much lower than of an UC case. In the first solution, the power is handled between the FES and the battery at 5.25 s as it is shown in Fig. 17. At the beginning of the simulation, the FW is capable of delivering all the power, having an increasing slope (along with the increase of vehicle speed). The vehicle power is less than the delivered power by the motors, this is due to the rolling friction forces at the wheels and drag resistance as the vehicle gains speed. At time 5.25 s, the battery helps the FES in delivering power. In fact, with the decreasing of the FW rotational speed, the FES has a diminishing capability facing to an increasing power demand. In that case, the battery helps, in parallel, the FW in delivering the needed power. As for the second solution, at the time the UC is completely discharged,

Table 17
Start-up on an asphalt dry road - FES as secondary energy storage.

SOE (%)	Energy delivered (kJ)		Battery intervention time	Battery current peak (A)
	Flywheel	Battery		
100	114.6	0.006	X	X
75	114.6	0.006	X	X
50	114.6	0.006	X	X
25	111.89	2.48	Starting at 5.2 s	17 A
10	94.8	19.57	Starting at 4 s	104 A

Table 18
Start-up on an asphalt dry road - UC as secondary energy storage.

SOE (%)	Energy delivered (kJ)		Battery intervention time	Battery current peak (A)
	UC	Battery		
100	118.9	0	X	X
75	119.7	0	X	X
50	121.6	0	X	X
25	96.9	19.17	Starting at 5.14 s	85.18 A
10	40.4	73.2	Starting at 3.37 s	104.7 A

Table 19
Start-up on a cobblestone wet road - FES as secondary energy storage.

SOE (%)	Energy delivered (kJ)		Battery intervention time	Battery current peak (A)
	Flywheel	Battery		
100	113.3	0.006	X	X
75	113.3	0.006	X	X
50	113.3	0.006	X	X
25	111.1	2.24	Starting at 5.25 s	16.2 A
10	94.8	18.54	Starting at 4.1 s	103.8 A

Table 20
Start-up on a cobblestone wet road - UC as secondary energy storage.

SOE (%)	Energy delivered (kJ)		Battery intervention time	Battery current peak (A)
	UC	Battery		
100	117.98	0	X	X
75	118.76	0	X	X
50	120.79	0	X	X
25	101	15.2	Starting at 5.4 s	105.8 A
10	40.4	72.7	Starting at 3.37 s	104 A

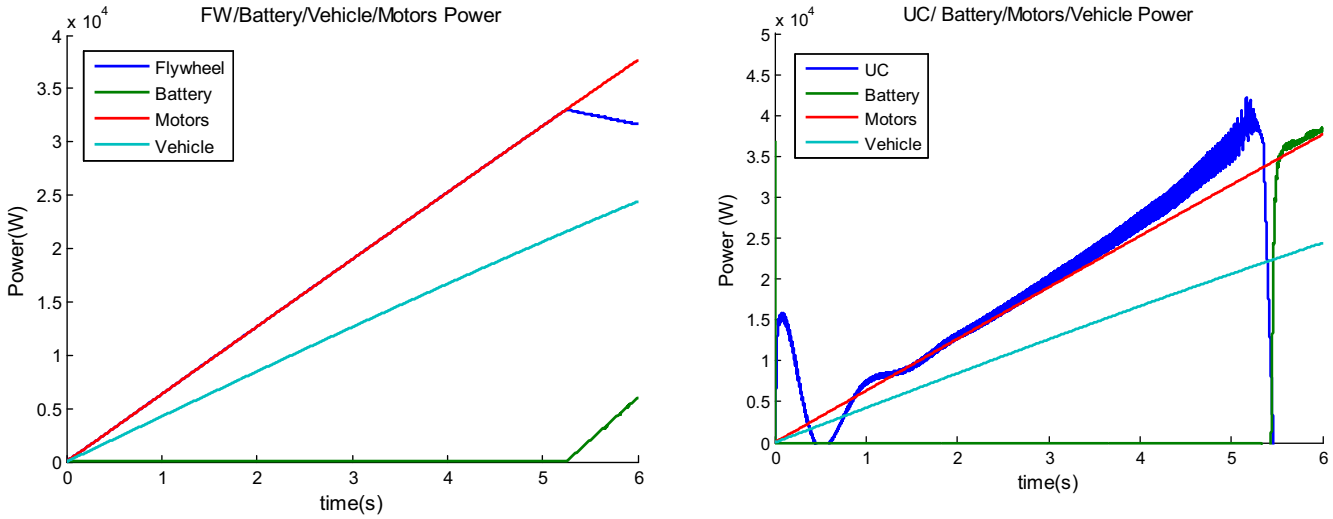

Fig. 17. Power profiles for different elements in the case of traction of the vehicle on a cobblestone wet road type - SOE = 25%.

SOE reaches 0% at time t = 5.4 s. The battery is forced to handle all the power (34.6 kW) which explains the high value of current equal to 105.8 A at the end of the simulation.

7. Conclusion

The paper proposes the comparative study of two hybrids energy storage system (HESS) of a two front wheel driven electric vehicle. The primary energy storage is a Li-Ion battery, known for its high energy density. Whereas the secondary energy storage could be either an UC or a FES, chosen for their high power densities and cycle life. The main objective is to reduce the battery intervention during vehicle regenerative braking or start up in order to enhance its cycle life and conserve its capacity performance, as well as to respond to the vehicle dynamic power requirements during extreme braking and traction operations. Due to the important number of UC manufacturers available on the market, a wide range of UC specifications is available for design and selection purposes. Whereas for FES, a more detailed design study should be performed. A techno-economic comparative study is ensured. According to an optimized design for FES relative to the particular two-front wheel driven electric vehicle application, results show that the FES is more advantageous than the UC solution in terms of volume, energy density, power density and even cost. When in fact, the use of UC is encouraged if weight, specific energy and specific power are major selection criteria. In a second stage, each HESS is integrated in a more global system including the vehicle, the braking and traction control systems and the driven motors. Tests are performed on two different surface road types and conditions (high and low friction roads) and for different initial states of charge. In respect of battery constraints minimization and its lifespan longevity preservation, if the energy management system of the vehicle requires the discharging of the secondary energy storage element in order to recover the braking energy while driving, the use of UC is by far much more convenient than the use of a FES. For traction tests, if the energy management system requires the secondary energy storage element charging before start up, the two HESS solutions give similar conclusions.

References

[1] Sierzchula William, Bakker Sjoerd, Maat Kees, van Wee Bert. The competitive environment of electric vehicles: an analysis of prototype and production models. Environ. Innov. Soc. Trans. 2012;2:49–65. Elsevier.

[2] Timmermans Jean-Marc, Nikolian Alexandros, De Hoog Joris, Gopalakrishnan Rahul, Goutam Shovon, Omar Noshin, et al. Batteries 2020 — Lithium-ion battery first and second life ageing, validated battery models, lifetime modelling and ageing assessment of thermal parameters. In: 18th European conference on power electronics and applications (EPE'16 ECCE Europe). IEEE; 2016.

[3] International Energy Agency. International Technology Perspectives 2008 — scenarios and strategies to 2050; 2008.

[4] World Bank. The cost of air pollution: strengthening the economic case for action. Washington: The World Bank and Institute for Health Metrics and Evaluation; 2016.

[5] Boughriet R. Véhicules électriques: un Livre Vert pour développer les infrastructures de recharge publiques 27 Avril 2011. Available: <http://www.actu-environnement.com/ae/news/livre-vert-recharges-voitures-electriques-collectivites-louis-negre-12454.php4>; 2011 [Accessed 19 August 2016].

[6] Tesla. Giga Factory Available: <https://www.tesla.com/fr_FR/gigafactory>; 2016.

[7] WhiteHouse.gov. FACT SHEET: Obama Administration Announces Federal and Private Sector Actions to Accelerate Electric Vehicle Adoption in the United States 21 July 2016. Available: <http://energy.gov/articles/fact-sheet-obama-administration-announces-federal-and-private-sector-actions-accelerate>; 2016.

[8] Durable D. Loi Grenelle 2 Available: <http://www.developpement-durable.gouv.fr/IMG/pdf/Grenelle_Loi-2.pdf>; Novembre 2010 [Accessed 10 August 2016] [in French].

[9] Durable D. Vers une mobilité Automobile Durable Juin 2013. Available: <http://www.developpement-durable.gouv.fr/IMG/pdf/Revue_du_CGDD_24_07_2013.pdf>; 2013 [Accessed 10 August 2016] [in French].

[10] Monnier P. Mercedes s'apprêterait à lancer toute une gamme de véhicules électriques 05 August 2016. Available: <http://www.usinenouvelle.com/article/mercedes-s-appreterait-a-lancer-toute-une-gamme-de-vehicules-electriques.N422317>; 2016 [in French].

[11] Kapoor Radhika, Perveen Mallika. Comparative study on various KERS. Proceedings of the world congress on engineering 2013, London, UK, vol. III.

[12] Boicea Valentin A. Energy storage technologies: the past and the present. Proc IEEE 2014;102(11):1777–94.

[13] Daoud Mohamad, Abdel-Khalik AS, Massoud A, Ahmed S, Abbasy NabilH. On the development of flywheel storage systems for power system applications: a survey. In: XXth international conference on electrical machines. IEEE; 2012. p. 2119–25.

[14] Amirante Riccardo, Cassone Egidio, Distaso Elia, Tamburrano Paolo. Overview on recent developments in energy storage: mechanical, electrochemical and hydrogen technologies. Energy Convers Manage 2017;132:372–87.

[15] Hedlund M, Lundin J, de Santiago J, Abrahamsson J, Bernhoff H. Flywheel energy storage for automotive applications. Energies 2015;8:10636–63.

[16] Dhand A, Pullen KR. Optimal energy management for a flywheel-assisted battery electric vehicle. Proc Inst Mech Eng D J Automob Eng 2015;229(12):1672–82.

[17] Dhand Aditya. Design of electric vehicle propulsion system incorporating flywheel energy storage Unpublished Doctoral thesis. City University London; 2015.

[18] He Jianhui, Ao Guoqiang, Guo Jinsheng, Chen Ziqiang, Yang Lin. Hybrid electric vehicle with flywheel energy storage system. WSEAS Trans Syst 2009;8(5):638–48.

[19] Streit Lubos, Talla Jakub. Energy storage savings depended on recuperation ratio in traction. ELEKTRO, IEEE; 2016.

[20] Ciccarelli Flavio. Energy management and control strategies for the use of supercapacitors storage technologies in urban railway traction systems PhD Thesis. PhD School in Industrial Engineering, University of Naples "Frederico II"; March 2014.

[21] Ratniyomchai Tosaphol, Hillmansen Stuart, Tricoli Pietro. Recent developments and applications of energy storage devices in electrified railways. Inst Eng Technol, Elect Syst Transp 2014;4(1):9–20.
[22] Qiua Chengqun, Wang Guolin. New evaluation methodology of regenerative braking contribution to energy efficiency improvement of electric vehicles. Energy Convers Manage 2016;119(1):389–98.
[23] Cibulka J. Kinetic energy recovery system by means of flywheel energy storage. Adv Eng 2009;3(1). ISSN 1846–5900.
[24] Pullen Kelth, Dhand Aditya. Characterization of flywheel energy storage system for hybrid vehicles. In: SAE 2014 world congress & exhibition, 2014, Detroit, USA.
[25] Holler Gert. Flywheel systems in automotive applications: design criteria, challenges, and effects on mobile energy storage systems. In: A3PS conference, Vienna.
[26] Plomer J, First J. Flywheel energy storage retrofit system for hybrid and electric vehicles. In: Smart cities symposium. Prague: IEEE; 2015.
[27] Daberkow Andreas, Ehlert Marcus, Kaise Dominik. Electric car operation and flywheel energy storage. In: Lienkamp M, editor. Conference on future automotive technology. Fachmedien Wiesbaden: Springer; 2013. p. 19–28.
[28] Lambert Timothy N, Washbum Cody M, Davis Danae J, Strong Jennifer, Massey Lee, Anderson Ben, et al. Next generation composite materials for flywheel development. Sandia National Laboratories; 2012.
[29] Hearn Clay, Thompson Richard, Pratap Sid, Lewis Michael, Chen Dongmel, Longoria Raul. Design of advanced flywheel energy storage for increasing penetration of intermittent renewable energy sources. The Center for Electromechanics and the Department of Mechanical Engineering, University of Texas, Austin.
[30] Olivier Jean-Christophe, Bernard Nicolas, Trieste Sony, Mendoza Luis, Bourguet Salvy. Techno-economic optimization of flywheel storage system in transportation. In: Symposium de Génie Electrique (SGE) 2014, Cachan, France.
[31] Trieste S, Hmam S, Olivier J-C, Bourguet S, Loron L. Technico-economic optimization of a supercapacitor-based energy storage unit chain: application on the first quick charge plug-in-ferry. Appl Energy 2015;153:3–14.
[32] Doucette RT, McCulloch MD. A comparison of high-speed flywheels, batteries, and ultracapacitors on the bases of cost and fuel economy as the energy storage system in a fuel cell based hybrid electric vehicle. J Power Sources 2011;196:1163–70.
[33] Elsayed Ahmed T, Mohammed Osama A. A comparative study on the optimal combination of hybrid energy storage system for ship power systems. In: Electric Ship Technologies Symposium (ESTS). IEEE; 2015. p. 140–5.
[34] Fernão Pires V, Romero-Cadaval Enrique, Vinnikov D, Roasto I, Martins JF. Power converter interfaces for electrochemical energy storage systems – a review. Energy Convers Manage 2014;86:453–75.
[35] Farhadi Mustafa, Mohammed Osama. Energy storage technologies for high power applications. IEEE Trans Ind Appl 2015.
[36] Wang Lei, Collins Ammanuel G, Li Hui. Optimal design and real-time control for energy management in electric vehicles. IEEE Trans Vehicular Technol 2011;69(4).
[37] Kenan Döşoğlu M, Arsoy Ayşen Basa, Güvenç Ugur. Application of STATCOM-supercapacitor for low-voltage ride-through capability in DFIG-based wind farm. Neural Comput Appl 2016:1–10.
[38] Abbey Chad, Joos Géza. Supercapacitor energy storage for wind energy applications. IEEE Trans Ind Appl 2007;43(3):769–76.
[39] Kenan Döşoğlu M, Arsoy Ayşen Basa. Transient modeling and analysis of a DFIG based wind farm with supercapacitor energy storage. Elect Power Energy Syst 2016;78:414–21.
[40] Guo Wenyong, Xiao Liye, Dai Shaotao. Enhancing low-voltage ride-through capability and smoothing output power of DFIG with a superconducting fault-current limiter-magnetic energy storage system. IEEE Trans Energy Convers 2012;27(2):277–95.
[41] Walsh John, Muneer Tariq, Celik Ali N. Design and analysis of kinetic energy recovery for automobiles: case study for commuters in Edinburgh. J Renew Sustain Energy 2011;3:013105–11. American Institute of Physics.
[42] Cherry Jeff. Battery durability in electrified vehicle applications: a review of degradation mechanisms and durability testing. Environmental Protection Agency; 2015. Final Report EP-C-12-014 WA 3-01, August 7.
[43] Castaings Ali, Lhomme Walter, Trigui Rochdi, Bouscayrol Alain. Comparison of energy management strategies of a battery/supercapacitors system for electric vehicle under real-time constraints. Appl Energy 2016;163:190–200.
[44] Bender Donald. Flywheels. Sandia National Laboratories; 2015. SAND2015-3976.
[45] Sepe Raymond B, Steyerl Anton, Batien Steven P. Lithium-ion supercapacitors for pulsed power applications. In: Energy conversion congress and exposition. IEEE; 2011. p. 1813–8.
[46] Beardsall Jamie C, Gould Christopher A, Al-Tai Moofik. Energy storage systems: a review of the technology and its application in power systems. In: 50th International Universities Power Engineering Conference (UPEC). IEEE; 2015. p. 1–6.
[47] Ronsmans Jan, Lalande Benoit. Combining energy with power: lithium-ion capacitors. In: IEEE, international symposium on power electronics, electrical drives, automation and motion. IEEE; 2016. p. 261–4.
[48] Foley Ian. Williams hybrid power—flywheel energy storage Presentation <http://www.ukintpress-conferences.com/uploads/SPKPMW13R/d1_s1_p2_ian_foley.pdf>; 2013 [accessed on 22 November 2016].
[49] An Assessment of Flywheel High Power Energy Storage Technology for Hybrid Vehicles, report n° ORNL/TM-2010/280, managed by UT-BATTELE for the Department of Energy, Oak Ridge National Laboratory, December 2011.
[50] Sharma Pawan, Bhatti TS. A review on electrochemical double-layer capacitors. Energy Convers Manage 2010;51(12):2901–12.
[51] Chemali E, Peindl M, Malysz P, Emadi A. Electrochemical and electrostatic energy storage and management systems for electric drive vehicles: state-of-the-art review and future trends. IEEE J Emerg Select Topics Power Electron 2016;4(3):1117–34.
[52] Review of ELV Exemption 5: From the view of Lithium-Ion battery makers and experts. A123 Systems LLC, Fraunhofer ICT, LG Chem Ltd and Samsung SDI Co., Ltd, December 2014.
[53] Ehsani Mehrdad, Gao Yimin, Emadi Ali. Modern electric, hybrid electric, and fuel cells vehicles. Taylor and Francis Group, LLC, CRC Press; 2010.
[54] Maxwell Technologies®; Document number: 3000489.1, <www.maxwell.com>.
[55] Itani K, De Bernardinis A, Khatir Z, Jammal A, Ouiedat M. Regenerative braking modeling, control, and simulation of a hybrid energy storage system for an electric vehicle in extreme conditions. IEEE Trans Transport Elect 2016;2(4):465–79.
[56] Itani K, De Bernardinis A, Khatir Z, Jammal A, Oueidat M. Control strategy for extreme conditions regenerative braking of a hybrid energy storage system for an electric vehicle. In: INDIN 2016, IEEE International Conference on Industrial Informatics, Poitiers, France, 18-21 July 2016.
[57] Itani K, De Bernardinis A, Khatir Z, Jammal A. Energy management of a battery-flywheel storage system used for regenerative braking recuperation of an electric vehicle. In: IEEE IECON 2016, Florence, Italy, 24-27 October 2016.
[58] Itani K, De Bernardinis A, Khatir Z, Jammal A. Comparison between two braking control methods, integrating energy recovery for a two-wheel front driven electric vehicle. Energy Convers Manage August 2016;122(15):330–43.
[59] Marques Maria Inês Lopes. Design and control of an electrical machines for flywheel energy storage system. Instituto Superior Técnico, dissertation submitted for obtaining the degree of Master in Electrical and Computer Engineer, Universidade Técnica de Lisboa; May 2008.
[60] Cleveland Cutler J, Morris Christopher. Handbook of energy, Volume I: Diagrams, charts, and tables. Elsevier; 2013. ISBN: 978-0-08-046405-3.
[61] Lipo TA. Introduction to AC machine design, vol. 1. Madison (Wisconsin, USA): University of Wisconsin; 1996.
[62] Agudelo Carlos E, Ferro E. Technical overview of brake performance testing for Original Equipment and Aftermarket industries in the US and European markets. Link technical report FEV2005-01, available at: <http://www.linkeng.com/>.
[63] ECE/324/Rev.1/Add.12/Rev.8, Addendum 12: Regulation No.13, Agreement Concerning the Adoption of Uniform Technical Prescriptions for Wheeled Vehicles, Equipment and Parts which can be Fitted and/or be Used on Wheeled Vehicles and the Conditions for Reciprocal Recognition of Approvals Granted on the Basis of these Prescriptions, United Nations, 3 March 2014, available at: <https://www.unece.org/fileadmin/DAM/trans/main/wp29/wp29regs/updates/R013r8e.pdf>.
[64] Hoàng TB, Pasillas-Lépine W, De Bernardinis A, Netto M. Extended braking stiffness estimation based on a switched observer, with an application to wheel-acceleration control. IEEE Trans Control Syst Technol 2014;22(6):2384–92.
[65] Project Group: MCE4-1024, Design of Slip-based Active Braking and Traction Control System for the Electric Vehicle QBEAK, Rune Wiben, Mads Hellegaard Andersen, Hans-Christian Becker Jensen, Master's Thesis, 157p. Aalborg University, 14 Jun 2012, publishing institution: AAU - Study of Energy.
[66] de Castro R, Araújo RE, Freitas D. Wheel slip control of EVs based on sliding mode technique with conditional integrators. IEEE Trans Ind Electron 2013;60(8):3256–71.
[67] Berger M, Côté O, Chebak A. Development of a DC-link protection system for regenerative braking of Electric Vehicle using a pseudo-cascade controlled IGBT chopper. In: Transportation Electrification Conference and Expo (ITEC). IEEE; 2015. p. 1–7.